Geofluids (2002) 2, 3–23

Gas breakthrough experiments on fine-grained sedimentary rocks

A. HILDENBRAND[1], S. SCHLÖMER[2,*] AND B. M. KROOSS[1]

[1]*Lehrstuhl für Geologie, Geochemie and Lagerstätten des Erdöls and der Kohle, Rheinisch-Westfälische Technische Hochschule (RWTH) Aachen, Germany;* [2]*EniTecnologie SpA, Via F. Maritano 26, San Donato Milanese, Italy*

ABSTRACT

The capillary sealing efficiency of fine-grained sedimentary rocks has been investigated by gas breakthrough experiments on fully water saturated claystones and siltstones (Boom Clay from Belgium, Opalinus Clay from Switzerland and Tertiary mudstone from offshore Norway) of different lithological compositions. Sand contents of the samples were consistently below 12%, major clay minerals were illite and smectite. Porosities determined by mercury injection lay between 10 and 30% while specific surface areas determined by nitrogen adsorption (BET method) ranged from 20 to 48 $m^2 g^{-1}$. Total organic carbon contents were below 2%.

Prior to the gas breakthrough experiments the absolute (single phase) permeability (k_{abs}) of the samples was determined by steady state flow tests with water or NaCl brine. The k_{abs} values ranged between 3 and 550 nDarcy (3×10^{-21} and 5.5×10^{-19} m^2). The maximum effective permeability to the gas-phase (k_{eff}) measured after gas breakthrough on initially water-saturated samples extended from 0.01 nDarcy (1×10^{-23} m^2) up to 1100 nDarcy (1.1×10^{-18} m^2). The residual differential pressures after re-imbibition of the water phase, referred to as the 'minimum capillary displacement pressures' (P_d), ranged from 0.06 to 6.7 MPa. During the re-imbibition process the effective permeability to the gas phase decreases with decreasing differential pressure. The recorded permeability/pressure data were used to derive the pore size distribution (mostly between 8 and 60 nm) and the transport porosity of the conducting pore system (10^{-5}–10^{-2}%).

Correlations could be established between (i) absolute permeability coefficients and the maximum effective permeability coefficients and (ii) effective or absolute permeability coefficients and capillary sealing efficiency. No correlation was found between the capillary displacement pressures determined from gas breakthrough experiments and those derived theoretically by mercury injection.

Key words: capillary processes, fine-grained lithologies, gas breakthrough, imbibition, sealing efficiency

Received 30 August 2001; accepted 24 January 2002

Corresponding author: B. M. Krooss, Lehrstuhl für Geologie, Geochemie und Lagerstätten des Erdöls und der Kohle, Rheinisch-Westfälische Technische Hochschule (RWTH) Aachen, Lochnerstr. 4–20, D-52056-Aachen, Germany.
E-mail: krooss@lek.rwth-aachen.de. Tel: +49 241 80 95753. Fax: +49 241 80 92152.

Geofluids (2002) **2**, 3–23

INTRODUCTION

Fine-grained (pelitic) rocks (clays, claystones, shales, mudrocks, siltstones) represent the major inventory of sedimentary basins. Their horizontal and vertical distribution and continuity determines the local and regional fluid flow processes and patterns on the geological time scale.

Pelitic rocks usually act as potential flow barriers and seals because fluid transport within and across them proceeds at low rates and efficiencies. These properties are considered beneficial in the context of petroleum and natural gas exploration and increasingly so in the search for repositories to sequester waste (radioactive and nonradioactive) from the human environment for extended ('geologic') periods of time. Storage of CO_2 from anthropogenic emissions in the subsurface has recently become another issue focusing research interest on the retention/sealing efficiency of fine-grained sedimentary rocks.

*Present address: GeoForschungsZentrum Potsdam, Telegrafenberg, D-14473, Potsdam, Germany

The poor fluid conductivity of pelitic rocks can also lead to the formation of overpressure zones in the subsurface which may constitute a hazard during petroleum exploration and production activities.

The measurement of petrophysical and fluid transport properties of fine-grained rocks is time-consuming and the corresponding data base is relatively small. The large variability in mineralogical compositions of naturally occurring shales, claystones, etc. poses an additional problem in the quantitative assessment and prediction of fluid transport processes and sealing efficiency. For example, absolute permeability coefficients may range over three orders of magnitude for a given porosity (Neuzil 1994).

Over the past decade our group has compiled a database of petrophysical, mineralogical and geochemical parameters for various fine-grained rocks. The basic transport processes that have been investigated in various studies were the pressure-driven volume flow and the molecular diffusion of hydrocarbon and nonhydrocarbon gases through water-saturated rocks (Schlömer & Krooss 1997; Schlömer 1998; Zhang & Krooss 2001). Pore-size distributions have been determined routinely on a large number of samples by mercury porosimetry.

More recently, the focus of interest has shifted to *two-phase* fluid flow processes in fine-grained sedimentary rocks. While multiphase fluid flow has been studied extensively in coarse-grained sedimentary systems like reservoir rocks and unsaturated soils, only very little is known about these processes in shales and claystones.

For natural gas exploration and the deposition of radioactive waste, the gas sealing efficiency of shales is an important parameter which has been studied using different approaches (Ibrahim *et al.* 1970; Schowalter 1979; Horseman *et al.* 1999). Apart from the displacement pressure required to force a gas phase into the initially water-saturated pore system of a mudstone, the quality of a seal is characterised by the effective permeability to the gas-phase after breakthrough. The effective permeability is a function of the gas/water saturation of the conducting pore system which, however, cannot be readily determined or controlled in fine-grained (pelitic) rocks. In the present study, gas breakthrough experiments have been performed providing information both on the capillary sealing efficiency and the effective gas permeability of mudrocks after gas breakthrough. The experimental procedure, evaluation method and results are documented and discussed in the following sections.

Fluid Transport Processes (Terms and Definitions)

Single-phase flow

Single phase fluid flow through a porous medium (rock, sedimentary column) is described by Darcy's law (See Appendix, eq. B3). The absolute permeability coefficient (k_{abs}) relates the flux (Q) of a fluid of a given viscosity (η) to the pressure gradient (ΔP) acting as the driving force of this transport process. It is a characteristic parameter of a rock that determines how easily a fluid of a given viscosity moves through it.

Two-phase flow

The dominant transport mechanism in hydrocarbon migration and dismigration is separate phase fluid flow (Darcy flow), either through matrix porosity or fracture networks. In the presence of two or more immiscible fluid phases in a porous rock, two-phase or multiphase flow will occur which is associated with capillary effects. Fluid transport is then controlled by the interfacial tension of the fluids involved, the wettability of the solid surface (wetting angle) with respect to the fluids, and the structure of the pore system. According to the Washburn equation (Washburn 1921) intrusion of a nonwetting fluid into a cylindrical capillary of radius r occurs only if the capillary pressure P_c (i.e. the pressure difference between the two immiscible fluids) within a pore is exceeded:

$$P_c = P_2 - P_1 = (2\gamma \cos\theta)/(r) \quad (1)$$

Here γ is the interfacial tension [$N\,m^{-1}$], and θ the wetting angle [degrees] and r is the radius [m] of the ideal cylindrical pores.

Capillary sealing efficiency and breakthrough pressure. The stages of the capillary breakthrough process of a nonwetting fluid through a porous medium are shown schematically in Fig. 1. The capillary sealing efficiency of a porous medium with a heterogeneous pore system (i.e. a given pore-size distribution) is characterised by the 'breakthrough pressure' ($P_{c,\,breakthrough}$) or 'threshold pressure' ($P_{c,\,threshold}$). This term refers to the excess pressure in the nonwetting phase at which the wetting phase is displaced to an extent that the percolation threshold is exceeded and continuous flowpaths of nonwetting phase form across the pore system. These flowpaths will comprise the largest interconnected pores, which offer the least resistance to capillary displacement. At this stage the flow of the nonwetting phase will be focused and restricted to a small portion of the interconnected pore system. If the excess pressure increases further, additional fluid flow pathways will develop across the porous medium, thus increasing the effective permeability to the nonwetting phase and the nonwetting phase saturation. The flowpaths will become less focused (flowpath divergence increases) and the fluid flow regime changes from capillary dominated to viscous dominated (Carruthers 1998). Thereby, each flowpath through the pore system is characterised by an effective pore radius (r_{eff}) corresponding to the narrowest pore throat along the entire path and a corresponding capillary pressure that has to be overcome to open the pathway.

Prior to reaching the threshold pressure a partial saturation of the pore system with the nonwetting fluid will occur once the excess pressure in this phase exceeds the capillary entry

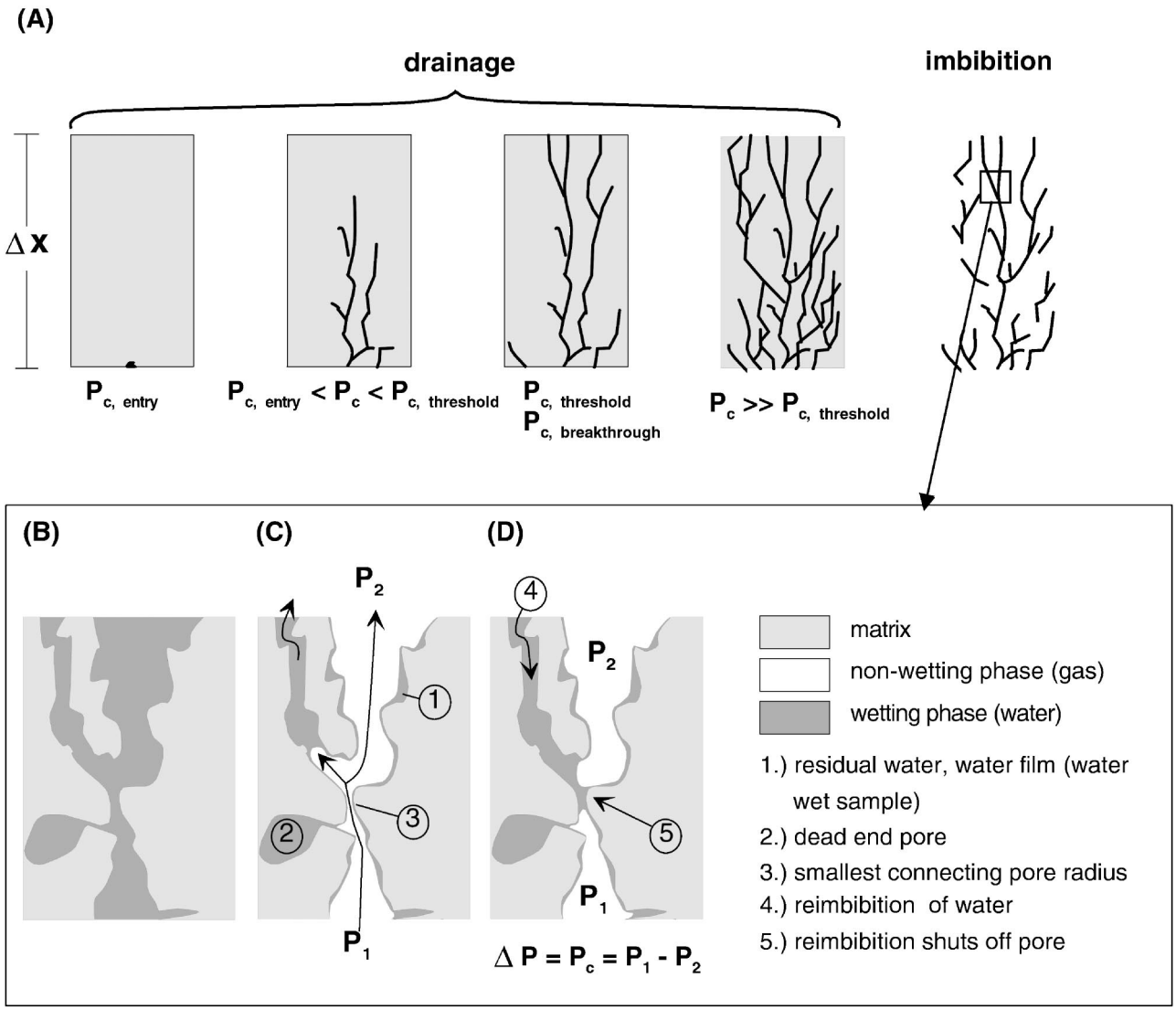

Fig. 1. (A) Stages of capillary gas breakthrough (drainage) and re-imbibition process in fine-grained rocks (schematic re-imbibition); (B) initially water-saturated sample; (C) gas breakthrough (D) re-imbibition.

pressure ($P_{c,\,entry}$), i.e. a pressure sufficiently high to force this fluid into the largest (but not interconnected) pores.

A reduction of the excess pressure in the nonwetting phase after gas breakthrough will lead to re-imbibition of the wetting phase, starting with the smallest pores and proceeding successively to larger pores. This process results in a continuous decrease in permeability (and relative permeability) for the nonwetting phase due to successive loss of interconnected flow-paths. Ultimately, when the last interconnected flow-path is shut off, the permeability for the nonwetting phase will drop to zero. Due to this loss of connectivity a pressure difference will persist between the gas phases below and above the seal. The absolute value of this pressure difference is a measure of the largest effective pore radius (r_{eff}) of the sample which determines the capillary sealing efficiency of the rock. During the re-imbibition process certain gas-filled pores may become isolated when the flow pathways are interrupted, resulting in a residual saturation.

Effective permeability and relative permeability. A porous rock containing two different, immiscible fluids has an effective permeability (k_{eff}) to each fluid phase as a function of its saturation. At 100% saturation the effective permeability equals the absolute permeability (k_{abs}) which should ideally be independent of the fluid phase. The ratio of the effective and the absolute permeability is the relative permeability (k_r) of the corresponding phase. During a drainage process the nonwetting fluid will occupy the larger and central part of the pores, having, at a similar degree of saturation, a comparatively higher relative permeability than the wetting fluid.

In the gas breakthrough experiments presented here, only the effective permeability for the gas phase could be

monitored as a function of the pressure gradient across the rock sample. Consequently, effective permeabilities for water are not reported.

Previous work on the gas sealing capacity of sedimentary rocks

Several previous studies have investigated the capillary sealing capacity of sedimentary rocks by using a nonwetting phase (usually a gas phase) to displace the wetting phase (usually water) from an initially completely saturated porous medium. Depending on the experimental procedures, interpretations and evaluations, different terminologies have been employed to denote characteristic gas pressures describing the capillary sealing efficiency. Table 1 gives an overview of various terms and definitions found in the literature.

A detailed literature review on this issue was already performed by Rodwell *et al.* (1999). In their discussion on capillary pressure (laboratory versus in-situ measurements) the data compilation of Ibrahim *et al.* (1970) was used, cited from Ingram *et al.* (1997). The pressure data reported by the latter authors, however, were converted from gas-water to mercury-air capillary pressures (Urai, personal communication 2001) and thus approximately one order magnitude higher than the original values for the system gas-water.

Table 2 summarizes correlations based on the present literature review. Note, that in the following text all pressure values used for correlations and in figures are symbolized by P_d (displacement pressure) for the gas-water system.

Thomas *et al.* (1968) performed measurements on eight samples, consisting of sand and limestones. Samples were 38 mm in diameter and 17–72 mm in length. Breakthrough experiments were performed under confining pressures from 6.9 up to 10.3 MPa. Gas (nitrogen) pressure was increased step-wise and the average water flow from the core was measured after each increment until flow ceased. When the threshold pressure was reached, a continuous flow of water resulted, ultimately followed by a free gas phase. Upon reduction of the gas pressure re-imbibition of the water was found to occur resulting in a resealing of the samples.

Table 1 Terms and definitions for threshold capillary entry pressures; For simplification the residual pressure difference determined in this study and pressure data obtained from other studies were denoted as P_d (displacement pressure).

Terminology	Definitions	Author
minimum displacement pressure (P_d)	residual pressure difference measured in nonsteady state experiments ($P_{c,\,residual}$) after re-imbibition of the wetting phase, i.e. pressure at which the nonwetting phase is displaced from the largest interconnected pores	this study
threshold displacement pressure	minimum differential pressure between the nonwetting phase and the wetting phase at which the gas starts to move continuously through the rock	Ibrahim *et al*. (1970)
capillary retention pressure (PCR)	pressure differential between the *in situ* pressure of the gas phase and the *in situ* pressure of the water phase above the gas at the gas-water interface in the caprock	Ibrahim *et al*. (1970)
threshold pressure	injection pressure at which a continuous flow of water resulted, and if enough time was allowed gas finally appeared at the outlet end of the core	Thomas *et al*. (1968)
displacement or breakthrough pressure	the minimum gas (injection) pressure required to establish a connected hydrocarbon filament through the largest interconnected water-saturated pore throats of the rock	Schowalter (1979; according tos Smith (1966)
critical pressure	denoting a sudden gas bubble release through the outlet tubing; gas flow is already detectable below this pressure	Pusch *et al*. (1985)
pore entry pressure or critical pressure	pressure at which gas flow is detected on the downstream side; below this pressure no gas migration is possible	Gallé & Tanai (1998), Gallé (2000)
breakthrough pressure	'second threshold pressure' at which gas flow at the downstream side increases sharply	Gallé & Tanai (1998), Gallé (2000)
breakthrough presure	excess gas pressure ($P_{gas(inflow\ side)}$-$P_{water(outflow\ side)}$) at which leakage occurs by a sudden gas outflow; the breakthrough pressure is fractionally larger than the swelling pressure of the clay	Horseman *et al*. (1997, 1999), Horseman *et al*. 1999)
peas gas pressure or peak response	peak excess gas pressure occurring directly after breakthrough; probably indicative of some sort of fracturing process	Horseman *et al*. (1997, 1999), Horseman (1999)
apparent capillary pressure or apparent matric suction	excess gas pressure at the extrapolated asymptote of the decreasing pressure curve when injection was stopped; no gas flow has ever been detected below this pressure	Horseman & Harrington (1997), Horseman (1999)
Hg-injection: displacement pressure	capillary pressure at 10% saturation	Schowalter (1979), Schlömer & Krooss (1997)
Hg-injection: threshold pressure	defined graphically; corresponds to the inflection point at which the curve becomes convex upward	Katz & Thompson (1987)

Table 2 Correlations based on data from different literature sources and this study, relating the absolute permeability (k_{abs}) and the capillary displacement pressure (P_d); R^2 is the regression coefficient, n is the number of data points. The individual definitions from each study are listed in Table 1.

source	formula	R^2	n	Data Range k_{abs} [nDarcy]	Data Range P_d [MPa]
Ibrahim *et al*. (1970)	$\log(P_d/[\,\mathrm{MPa}]) = -0.33\cdot\log(k_{abs}/[\mathrm{nDarcy}]) + 0.91$	0.81	325	$8.7\cdot10^{-2}$–$3.9\cdot10^{9}$	0.0045–14
Converted to system Hg-air by Ingram *et al*. (1997)	$\log(P_d/[\,\mathrm{MPa}]) = -0.33\cdot\log(k_{abs}/[\mathrm{nDarcy}]) + 1.70$				
based on data from:					
'Project 26–47'	$\log(P_d/[\,\mathrm{MPa}]) = -0.21\cdot\log(k_{abs}/[\mathrm{nDarcy}]) + 0.86$	0.52	33	$8.7\cdot10^{-2}$–$2.1\cdot10^{3}$	0.55–14
Commercial data	$\log(P_d/[\,\mathrm{MPa}]) = -0.34\cdot\log(k_{abs}/[\mathrm{nDarcy}]) + 0.90$	0.38	252	$2.2\cdot10^{0}$–$3.8\cdot10^{4}$	0.17–6.2
Wyllie & Rose data	$\log(P_d/[\,\mathrm{MPa}]) = -0.57\cdot\log(k_{abs}/[\mathrm{nDarcy}]) + 2.93$	0.89	20	$8.2\cdot10^{6}$–$3.9\cdot10^{9}$	0.0045–0.1
Thomas *et al*. (1968)	$\log(P_d/[\,\mathrm{MPa}]) = -0.43\cdot\log(k_{abs}/[\mathrm{nDarcy}]) + 1.30$	0.99	9	$4.1\cdot10^{1}$–$1.8\cdot10^{5}$	0.1–4.5
Rudd & Neilsen	$\log(P_d/[\,\mathrm{MPa}] = -0.06\cdot\log(k_{abs}/[\mathrm{nDarcy}]) + 0.79$	0.26	11	$8.8\cdot10^{-1}$–$5.3\cdot10^{2}$	3.1–6.9
total data compilation including:	$\log(P_d/[\,\mathrm{MPa}]) = -0.3293\ \log(k_{abs}/[\mathrm{nDarcy}]) + 0.9017$	0.86	334	$8.7\cdot10^{-2}$–$3.9\cdot10^{9}$	0.0045–14
Schowalter (1979)			4	$6.0\cdot10^{4}$–$3.5\cdot10^{5}$	0.12–0.27
Pusch *et al*. (1985)			5	$1.0\cdot10^{0}$–$4.0\cdot10^{3}$	0.3–5.0
this study	$\log(P_d/[\,\mathrm{MPa}]) = -0.81\ \log(k_{abs}/[\mathrm{nDarcy}]) + 1.15$	0.71	11	$1\cdot10^{-2}$–$5.0\cdot10^{1}$	0.06–6.7

In the 'Project 26–47' Ibrahim *et al.* (1970) conducted gas breakthrough experiments by incremental pressure increase at the inlet side of the samples. Each pressure was held constant until an almost complete stop in fluid movement was observed at the outlet side. Initial gas pressures were chosen according to previously measured single phase permeabilities and varied between 0.1 and 16.9 MPa. The confining pressure was not varied in order to accompany the different gas pressures.

Direct measurements of displacement pressure were also conducted by Schowalter (1979) on chalk and sandstone. Nitrogen pressure was increased step-wise at the high pressure side and the resulting water flux was recorded at the downstream side of the samples. Constant and higher flow rates, occurring at a distinct gas pressure (displacement pressure), were interpreted to be the result of a continuous gas phase across the sample length.

Oedometer tests were performed by Pusch *et al.* (1985) on MX-80 bentonite, covering samples 50 mm in diameter and up to 30 cm in length. Swelling pressure, absolute water permeability, gas permeability before breakthrough (only partly), and the final breakthrough pressure were recorded. Breakthrough experiments were either performed with atmospheric or enhanced (water) pressure at the downstream side. At the inflow side gas pressure was raised in increments of 0.5–2 MPa and held constant for at least 5 days until breakthrough occurred. The major results of this study were, that the critical pressure is in the range of 0.3–21 MPa (9 experiments), which correlated with the swelling pressure. An earlier study by Pusch (1983) showed the hydraulic conductivity and gas conductivity to be in the same order of magnitude varying between 10^{-13} and 2×10^{-14} ms^{-1} ($\sim10^{-20}$–10^{-21} m^2).

Tanai *et al.* (1997) investigated permeabilities and gas breakthrough on compacted bentonite (synthetic Kunigel V1) and Fo-Ca-Clay (Paris basin, France) by unsaturated and saturated flow experiments. The former experiments were performed on samples with predefined water saturations (S_w) between 0 and 80%, the latter were carried out on completely water saturated samples followed by a stepwise gas pressure increase (0.5 MPa per 120 h) until breakthrough occurred. The apparatus used accommodated samples with 50 mm in diameter, and up to 50 mm in length. Argon was used for both experiments, and gas flow was measured at the downstream side at atmospheric pressure (soap-bubble flow meter). The main conclusions from this study were as follows: (i) The absolute permeability measured with argon ($S_w = 0\%$) was about five orders of magnitude higher than absolute water permeabilities ($S_w = 100\%$). This phenomenon is due to swelling of the bentonite in the presence of water, (ii) for water saturations of about 72% no more gas flow was detected (relative gas permeability = 0), i.e. the interconnected pore system was blocked by water, (iii) gas permeabilities from saturated state experiments were in the order of 10^{-18}–10^{-21} m^2 for Kunigel V1, and 10^{-18} m^2 for the Fo-Ca-Clay, (iv) the capillary breakthrough pressure increased with increasing dry density of clay specimen, (v) the capillary breakthrough pressure is similar to the swelling pressure (~0.5–4 MPa), and (vi) breakthrough pressures are reproducible, showing that pathways created by first breakthrough experiment were closed by re-saturation

Gallé & Tanai (1998) and Gallé (2000) conducted gas breakthrough experiments on a synthetic Ca-smectite clay with predefined water saturations from 70 to 100%, using the same experimental gas migration testing system as described in Tanai *et al.* 1997). Due to the long experimental

durations only a few measurements were performed with fully water-saturated clays. The authors report two 'threshold pressures', the first and lower value is termed 'pore entry pressure', and the second is referred to as the 'final breakthrough pressure'. For fully saturated samples both values were close to each other.

Horseman *et al.* (1997, 1999) and Harrington & Horseman (1999) performed gas (He) injection experiments to determine capillary displacement pressures on Tertiary Boom clay with water-content porosities of > 40%, and on a synthetic bentonite (MX-80 bentonite). The experiments were performed with a constant gas flow rate ($375\,\mu L\,h^{-1}$) resulting in a continuous increase of the gas pressure (0.1–$0.004\,MPa\,h^{-1}$; Figs 4,5,6 in Harrington & Horseman 1999). All injection experiments on the Boom Clay showed a breakthrough, and a peak gas pressure (fracture initiation), followed by a spontaneous negative transient when gas injection was stopped. The excess gas pressure or the apparent matric suction (residual differential pressure) was found by extrapolating the negative transient curve, which in some experiments was rather uncertain. Beneath the threshold pressure gas flow was never detected. Subsequent gas injection tests on the same sample resulted in lower breakthrough pressures. The authors suggest this to be due to the presence of bubbles or residual gas-filled voids left along the routes of gas migration together with possible fabric damage.

EXPERIMENTAL

Triaxial Flow Cell

The fluid flow measurements were performed in triaxial flow cells designed for confining pressures up to 50 MPa (500 bar), axial load of up to 100 kN and maximum temperatures up to 350°C. Figure 2 shows an illustration of the components of the flow cells and the sample arrangement. The cells accommodate cylindrical sample plugs of 28.5 mm diameter and a maximum length of approximately 30 mm.

Sample plugs are placed between two porous stainless steel disks and two stainless steel pistons equipped with boreholes for fluid introduction and removal. The outer surface of the sample/piston arrangement is sealed with a double-layered sleeve. The inner sleeve consists of lead (Pb) foil (0.15 mm thickness); for the outer layer either thin-walled copper (Cu) or aluminium (Al) tubes are used. Application of the confining pressure (D in Fig. 2) of at least 300 bar ensures a leak-tight seal around the sample plugs. The efficiency of the double-layered sleeve system has been tested extensively in gas diffusion experiments (e.g. Schlömer & Krooss 1997).

The same sample arrangement was used for both single phase permeability measurements and gas breakthrough experiments.

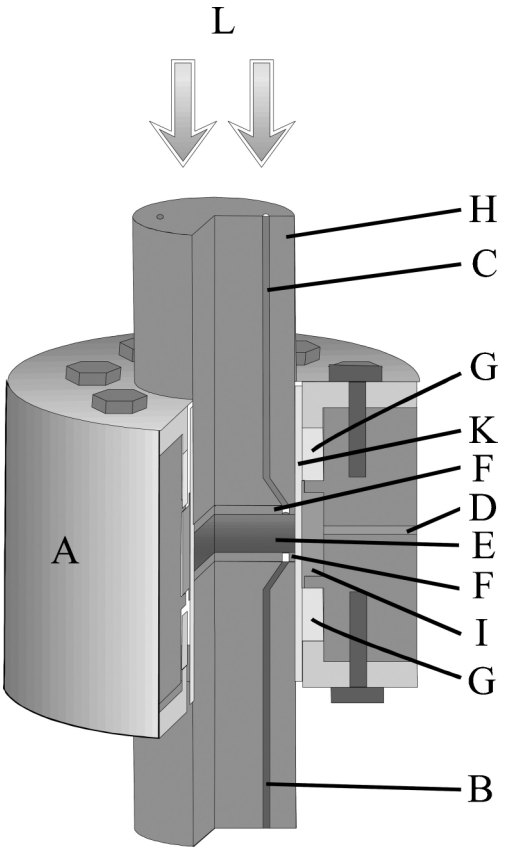

Fig. 2. Triaxial flow cell used for single-phase permeability measurements and gas breakthrough experiments. (A) stainless steel body; (B,C) 1/8 conduits; (D) connector for confining pressure; (E) cylindrical rock sample (28.5 mm diameter); (F) porous stainless steel disks (fluid reservoirs); (G) graphite packing material; (H) stainless steel pistons; (I) confining pressure compartment; (K) double-layered sleeve; (L) axial load.

Single-phase fluid flow measurements with water and brine

Single-phase experiments to determine the absolute permeability of the mudstones were performed with a steady-state method. Constant fluid pressure was applied at the upstream side and the fluid volume forced through the sample was measured at the downstream side of the pressure cell. The pressure at the downstream side was atmospheric. Normal tap water as well as brine (100 g NaCl/1 L H_2O) were used as fluid phases. With the exact diameter and length of the sample, the differential pressure, and the viscosity of the fluid known, Darcy's law was used to calculate the permeability of the rock sample.

Gas breakthrough experiments

The experimental procedure for gas breakthrough measurements applied in this study was chosen as a result of numerous tests exploring different approaches and configurations. Capillary breakthrough pressure of initially water-saturated rock specimens have been performed by various workers by

continuously increasing the pressure of the nonwetting fluid (gas) until breakthrough occurred (see above). While this approach was tested in our laboratory it became evident that application of gas pressures well above the anticipated threshold pressures in many instances resulted in a gas breakthrough only after days or even weeks. Due to this substantial time-lag, approaching the threshold pressure in small pressure increments would have resulted in prohibitively long durations of experiments. Likewise, an approach using a continuous pressure increase would have required an extremely low increase rate (and correspondingly long measuring periods) to avoid overshooting and an overestimation of threshold pressures. The dynamic aspects of capillary breakthrough in fine-grained rocks as reflected in the above-mentioned time-lag phenomena deserve particular attention in further studies.

Gas breakthrough experiments in this study were performed by imposing instantaneously a high gas-pressure gradient (i.e. exceeding the expected gas breakthrough pressure) across the rock samples and monitoring the resulting gas flux by means of the pressure changes (nonsteady state, capillary controlled experiments). Complete water-saturation of the pore system was required as a defined initial condition for the experiments. Therefore all samples were first subjected to single-phase flow tests (see above). After constant single-phase flow was registered for an extended period of time, complete water-saturation of the conducting pore system was assumed. In order to avoid hydrofracturing of the sample the confining pressure in all experiments was set to 30 MPa which was well above the initial gas pressures ($P_{c,\,initial} <$ 17 MPa).

The two experimental procedures used are shown schematically in Fig. 3. In both cases the volume of the downstream (low-pressure) side of the system was fixed. This volume consisted of the dead volume of the pressure transducer ($\sim$1 cm^3), the tubing and the pore volume of the stainless steel porous plate. The residual water from the preceding permeability tests was removed from the tubing and the porous steel disk by a gas current before the compartment was sealed. Small amounts of water in the porous steel plate were tolerated because they did not substantially affect the volumetrics of the system and were considered to provide a reservoir for the re-imbibition cycle.

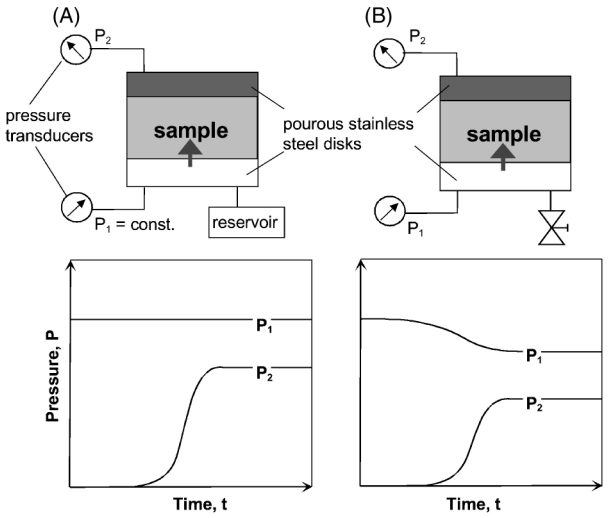

Fig. 3. Scheme of the two experimental modes used in this study. (A) constant pressure at upstream side; (B) introduction of gas into a fixed upstream volume; downstream volume fixed in both instances.

The upstream (high-pressure) side of the cell was either kept at a constant pressure by means of a pressure regulator (procedure A) or filled with gas at high pressure and then sealed (procedure B). The volumes of the two compartments typically ranged around 2–3 cm^3.

The breakthrough pressure curves resulting from the two procedures are shown schematically in Fig. 3. During procedure A the pressure in downstream chamber increases after a certain lag time and approaches the upstream pressure. Normally, a complete pressure equilibration between the two chambers is not reached, but a residual pressure difference remains which is a characteristic parameter for the rock sample analysed. In procedure B the pressure in the downstream chamber increases while the pressure in the upstream compartment decreases correspondingly. Here, too a residual pressure difference persists, however, at an intermediate pressure level depending on the relative volumes of the compartments. During the experiments the pressures in the upstream and downstream compartments and the system temperature were recorded continuously. The evaluation further required the instrument parameters (volumes of the upstream and downstream flow-cell chambers) and the geometry of the sample plugs (length, cross section area).

Effective permeability measurements

After gas breakthrough has occurred, a continuous gas flux will evolve from the high-pressure to the low-pressure compartment until the residual pressure gradient is reached. During the experiment the effective gas permeability (k_{eff}) of the sample varies with time as a function of water saturation. The effective permeability is calculated from the pressure change in the downstream compartment using Darcy's law for compressible media (see Appendix B for details):

$$k_{eff} = -\frac{V_2 \cdot \eta \cdot 2\Delta x}{A(P_2^2 - P_1^2)} \frac{dP_2}{dt}, \qquad (2)$$

where V_2 [m^3] is the volume of the downstream compartment and P_2 [Pa] the corresponding pressure, k [m^2] is the effective permeability to the gas phase, A [m^2] is the cross section area, [Pa s] is the viscosity of the gas, and Δx [m] is the length of the sample. In the experiments performed with method B (Fig. 3) the effective permeability was also determined from the pressure decline in the closed upstream compartment.

Mercury porosimetry

The petrophysical characterization of the pore system of the rock samples by mercury injection was performed using a QUANTACHROME AUTOSCAN 60 porosimeter. Measurements were carried out with cuttings (5–10 mm) dried at 105°C for 24 h. Capillary pressure curves were recorded at a constant pressure increase rate of 8.5 MPa min^{-1} from ambient pressure up to 345 MPa. Using the Washburn equation (Washburn 1921) with an interfacial tension value of $\gamma = 0.471$ Nm^{-1} and a wetting angle $\theta = 141°$, this capillary pressure converts to an equivalent pore radius (cylindrical capillaries) of about 2 nm.

Assessment of specific surface area

A Micromeritics GEMINI 2360 apparatus was used for the determination of the specific surface areas (S_0) of the rock samples. Measurements were performed with nitrogen on cuttings (1–2 mm in diameter) using the multipoint BET method. Prior to the measurements the samples were dried at 105°C for 24 h.

EVALUATION AND INTERPRETATION OF GAS BREAKTHROUGH EXPERIMENTS

The raw data obtained from the gas breakthrough experiments were evaluated and interpreted in terms of a conceptual model on capillary and fluid flow processes which is outlined in the following paragraphs.

Interpretation of experimental breakthrough curves

Figure 4 shows the typical results of a gas breakthrough experiment conducted according to procedure A (cf. Figure 3). The primary experimental data are the pressures in the upstream (P_1) and the downstream (P_2) compartments as a function of time. Also shown in this diagram is the differential pressure ($\Delta P = P_1 - P_2$) and the effective gas permeability (k_{eff}). Initially, only a slow pressure increase is observed in the downstream compartment of the arrangement. A massive gas breakthrough occurs only about 7–8 days after the start of the experiment. In the final phase of the experiment the gas flow stops and a constant pressure difference persists between the two compartments.

In Fig. 5 the relationships between the capillary processes and the experimental gas breakthrough curves (for experimental method B) are summarized schematically. The k_{eff} values, calculated from the pressure changes with time using Darcy's law for compressible media (see above) are shown as a function of experimental time in Fig. 5(a). They pass through a maximum and then decrease, as the pressure difference between the two compartments decreases towards the residual pressure difference $P_{c,\,residual}$.

It is important to note that gas breakthrough (drainage) under the experimental conditions used here occurs in an uncontrolled fashion after a substantial lag time which may range from hours to weeks. Thus, an equilibrium drainage curve (cf. curve I in Fig. 5b) yielding a distinct threshold pressure, at which the gas first migrates along a permeable pathway through the initially water-saturated sample, cannot be determined. Information on the capillary processes in the pelitic rock samples and the gas breakthrough characteristics can, however, be obtained from the interpretation of the spontaneous imbibition curve (curve II in Fig. 5b), when the water gradually displaces the gas-phase from the interconnected flowpaths.

Curve I in Fig. 5(b) is the conventional equilibrium drainage curve that would be obtained if the pressure of the non-wetting (gas) phase were increased continuously at a very low rate. At $P_{c,\,entry}$ gas starts to enter the pore system, causing a gradual reduction of water-saturation. When the pressure is further increased the percolation threshold is reached and capillary breakthrough occurs after $P_{c,\,threshold}$ (also denoted

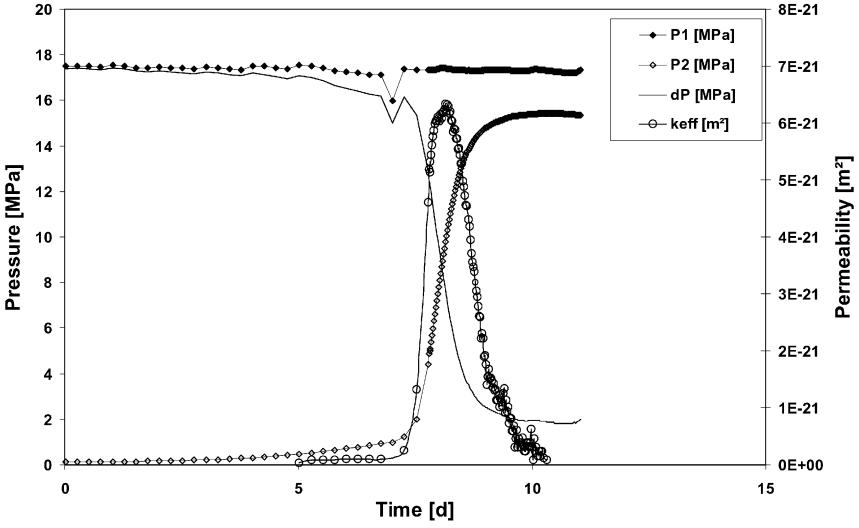

Fig. 4. Gas breakthrough curve for methane recorded with the experimental set-up using an initially water-saturated core plug. Shown are the pressures on the high-pressure and the low-pressure sides and the pressure difference between the reservoirs as a function of experiment time.

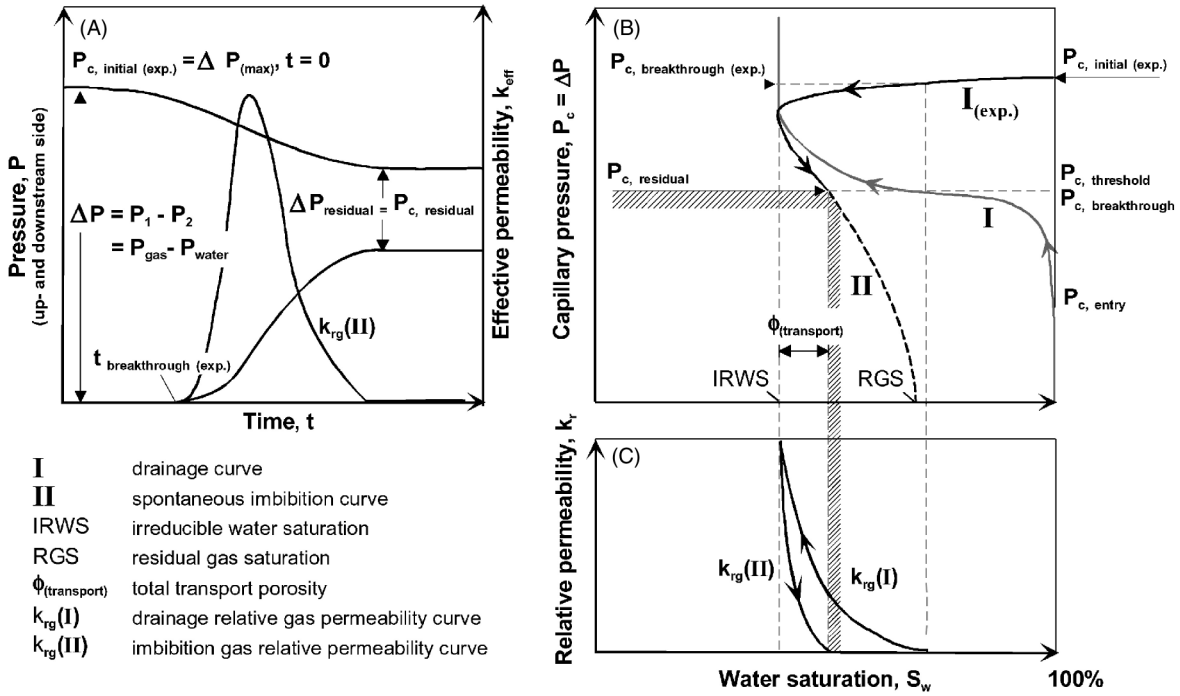

Fig. 5. Scheme of the experimental parameters recorded in this study and their interpretation in terms of capillary processes. (A) pressure history of a gas breakthrough experiment; (B) capillary pressure of the gas phase as a function of water saturation;. (C) relative permeability curve for the gas phase as a function of water saturation during drainage (I) and imbibition (II).

as $P_{c,\,breakthrough}$) is exceeded. Ultimately the equilibrium drainage curve approaches the Irreducible Water Saturation (IRWS) line.

The drainage curve corresponding to the *experimental procedure* used in the present study is denoted as $I_{(exp.)}$ in Fig. 5(b). It starts at complete water-saturation and an excess pressure $P_{c,\,initial\,(exp.)}$ well above the threshold pressure. Initially this pressure difference decreases only slowly (lag-time) until a rapid gas breakthrough ($P_{c,\,breakthrough\,(exp.)}$) occurs. This breakthrough is characterised by the corresponding steep increase in effective gas permeability (k_{eff}) at time $t_{breakthrough\,(exp.)}$ in Fig. 5(a). $P_{c,\,breakthrough\,(exp.)}$ in the $I_{(exp.)}$ curve is not a characteristic parameter of the porous medium but depends essentially on $P_{c,\,initial\,(exp.)}$. As the $I_{(exp.)}$ curve approaches the IRWS line, the effective gas permeability will increase and reach its maximum value (Fig. 5a) when the IRWS is reached. At this point drainage stops and, as the pressure difference (excess pressure) decreases, spontaneous imbibition (curve II) will start. This process is associated with an increase in water saturation and a reduction of the conducting flowpaths, resulting in a decrease of the effective (and relative) permeability to the nonwetting phase (cf. k_{rg}(II) in Fig. 5(b). Effective permeability will drop to zero and gas flow will stop when the imbibing water has shut off the last interconnected flowpath across the sample (i.e. the flowpath with the largest effective pore radius). The residual pressure difference ($P_{c,\,residual}$) maintained at this stage is also referred to as the minimum capillary displacement pressure (P_d). The hatched area below the $P_{c,\,residual}$ line in Fig. 5(b) indicates that the experimentally measured residual pressure difference may be lower than the 'true' value if reimbition is impeded. This will lead to an underestimation of the capillary sealing efficiency, while methods based on the drainage process will tend to overestimation.

The dotted portion of line (II) in Fig. 5(b), extending beyond the spontaneous imbibition line, corresponds to forced imbibition, which requires an increase in the wetting phase pressure.

The 'transport porosity' ($\phi_{transport}$) (conducting porosity) indicated in Fig. 5(b) corresponds to the portion of the pore system occupied by the interconnected gas flowpaths at IRWS. It extends from the IRWS to the end of the spontaneous imbibition curve and does not comprise the isolated and nonconducting gas-filled pores. The transport porosity can be estimated by means of a simple capillary model from the experimental gas breakthrough curves (see below).

Pore-volume distribution of the conducting pore system

An evaluation scheme based on a capillary bundle model has been used to quantify the experimental results in terms of a size distribution of the conducting equivalent pore system. This procedure uses the pressure and permeability data recorded during the spontaneous imbibition phase. The derivation of the scheme which is based on a combination of Darcy's and Poiseuille's laws is given in the Appendix B.

Table 3 Overview of mudrock samples used in this study.

Sample no.	Sample type	Depth [m]	Sample Origin
2000241	Tertiary mudstone	1580	Norwegian Shelf
2000242	Tertiary mudstone	1515	Norwegian Shelf
2000246	Opalinus Clay	250	Swiss Jura Mtns.
2000247	Boom clay	1053	Belgium (Molenbeersel)
2000251	Boom clay	1056	Belgium (Molenbeersel)
2000253	Boom clay	1057	Belgium (Molenbeersel)
2000254	Boom clay	220	Belgium (Mol)

SAMPLES

An overview of the mudstone samples investigated in this study is given in Table 3. The set comprises two Tertiary mudstone samples (2000241, 2000242) from wells located on the Norwegian Shelf, one Jurassic Opalinus Clay sample from Switzerland (Mont Terri Rock Laboratory, 2000246), three Tertiary (Early Oligocene) Boom Clay specimens from Molenbeersel (2000247, 2000251, 2000253), and one Boom Clay sample from Mol (2000254) in Belgium. The Norwegian samples cover a burial depth range from 1500 to 1600 m. The present overburden of the Mont Terri Rock Laboratory is 250 m, with an estimated former overburden of *c.* 1000 m (Thury & Bossart 1999). Boom Clay samples from Molenbeersel and Mol come from depths of ~1060 and 220 m, respectively.

The Boom Clay sample from Mol and samples from the Norwegian Shelf were well preserved in Al-PE (aluminium-polyethylene) bags and their original moisture content appeared well preserved upon reception (Table 4). The Opalinus Clay was supplied in two slabs (*c.* 10 kg) sealed in aluminium bags at the Mont Terri site. Despite these precautions the samples obviously had not maintained their original water-saturation but were also partly dried out. The core samples from the Molenbeersel had been stored in plastic bags in a core repository for 13 years and were dried out.

Mudstone specimens from the Norwegian Shelf were supplied by Norsk Hydro (Bergen), the Opalinus Clay was provided by NAGRA (National Cooperative for the Disposal of Radioactive Waste), and the Tertiary Boom Clay samples were made available by the Geological Survey of Belgium and by Prof. J. Urai of RWTH-Aachen.

Sample preparation

Plug preparation of the dried out core material caused serious problems because of the generally poor coherence of the samples. Standard techniques, like drilling of the plugs with a diamond drill bit, using water as cooling liquid, were unsuccessful. Ultimately, a conventional circular saw blade designed for drilling wood or metal was found to yield satisfactory results when used with dry samples. In some instances hand-trimming was necessary to obtain the required cylindrical shape.

Sedimentological and petrophysical characterization

Table 4 lists the sedimentological and petrophysical data of the samples studied in this project. The sand, silt and clay contents were determined according to the method of Odén (1916). Specifically the silt and clay percentages depend strongly on the preparation procedure used. Individual samples from this sequence were prepared according to the method of Tributh & Lagaly (1986) which removes compounds likely to cause aggregation of clay particles, i.e. Ca^{2+} ions, and bonding material like iron oxide and organic matter. This procedure generally resulted in substantially higher clay content values (not reported here). A discussion of the advantages and disadvantages of the various preparation methods and the usefulness of the resulting grain-size distributions for correlations concerning fluid transport properties is beyond the scope of this paper. The sand contents reported in Table 4 are consistently below 12% indicating that the sedimentological composition of the samples is dominated by fine-grained materials (silt and clay). Qualitatively, the major constituents of the clay fraction are illite and smectite with lesser amounts of kaolinite and chlorite.

The total organic carbon contents (TOC) of the Norwegian mudrocks, the Opalinus samples, and one Boom clay (2000247) are below 1% while values between 1 and 2% were found for the Boom clay samples 2000251, –253, and

sample no.	$\phi_{(Hg)}$ [%]	WC [%]	$\phi_{(WC)}$ [%]	sand content [%]	TOC [%]	TC [%]	BET S_0 [$m^2\,g^{-1}$]
2000241	26.1	16.1	34.0	12.1	0.2	0.2	30.56
2000242	29.9	19.8	42.8	10.5	0.6	0.6	26.21
2000246	10.3	–	–	6.3	0.8	1.9	26.8
2000247	24.4	–	–	7.4	0.9	0.9	20.1
2000251	23.5	–	–	10.0	1.6	1.7	23.6
2000253	23.4	–	–	7.7	1.7	2.1	20.6
2000254	24.0	17.7	35.8	0.5	1.2	1.3	48.2

Table 4 Petrophysical and sedimentological characteristics of samples used in this study; porosity determined from mercury injection ($\phi_{(Hg)}$), and from natural water content ($\phi_{(WC)}$), sand content total organic and total carbon content, and the specific surface area (BET-method).

Table 5 Results of mercury injection measurements; porosity values from mercury injection, $P_{d\ (Hg/air)}$ – mercury capillary displacement pressures taken at 10% saturation, $P_d^*{}_{(gas/water)}$ – gas/water displacement pressures calculated from Hg/air values, maxima of equivalent pore radius distributions from mercury porosimetry. Interfacial tensions: $\gamma_{(Hg/air)} = 480\ mN\ m^{-1}$, $\gamma_{(gas/water)} = 50\ mN\ m^{-1}$. Wetting angles: $\theta_{(Hg/air)} = 141°$, $\theta_{(gas/water)} = 0°$.

sample no.	ϕ [%]	$P_{d\ (Hg/air)}$ (10% saturation) [MPa]	$P_d^*{}_{(gas/water)}$ [MPa]	most prominent pore radius [nm]	second prominent pore radius [nm]
2000241	26.1	23.0	3.1	11	–
2000242	29.9	2.6	0.4	21	120
2000246	10.2	16.3	2.2	13	–
	10.4	14.9	2.0	13	3
2000247	24.4	0.3	0.0	740	25
	21.7	0.3	0.0	650	21
	23.5	0.3	0.0	780	15
2000251	23.5	0.8	0.1	20	270
2000253	23.4	0.7	0.1	21	350
2000254	24.0	15.5	2.1	30	–
average	22.1	6.8	0.9	211	193
minimum	10.2	0.3	0.0	11	3
maximum	29.9	23.0	3.1	780	740

−254. Total carbon contents indicate 1.1% carbonate for the Opalinus Clay and minor quantities of carbonate for Boom Clay.

Porosities determined by mercury injection are listed in Table 5. They range from 10% to 30% with the highest values found for the Tertiary mudrocks from the Norwegian shelf and the lowest value (10.3%) encountered for the Opalinus clay. Porosity values determined from the original water content (weight loss after drying at 105°C) were always significantly higher (34–43%) than those obtained by mercury injection. Also given in Table 5 are the capillary pressures, $P_{d(Hg/air)}$, at 10% mercury saturation which are commonly interpreted as breakthrough- or threshold pressures (Schowalter 1979). From these the corresponding pressures $P_d^*{}_{(gas/water)}$ for the gas/water system were computed. In the last two columns of Table 5 the most prominent and second prominent pore radii of the poresize distribution are reported.

Specific surface areas of the mudrocks, range from 20 up to 48 m^2/g with the highest value found for Boom clay sample 2000254 and the lowest value for one silty sample of the Boom Formation (2000247).

RESULTS

The results of the single phase (absolute) permeability measurements and the gas breakthrough experiments performed in this study are summarized in Table 6.

Absolute permeability

Absolute (single phase) permeabilities of the mudrock samples measured with water or brine solution range between 3 and 550 nDarcy (3×10^{-21}–5.5×10^{-19} m^2) (Table 6). The highest permeability coefficients were found for the Boom Clay, whereas the Opalinus samples and the Tertiary mudstones exhibited the lowest values.

In those cases where measurements were performed parallel and perpendicular to the bedding, a permeability anisotropy was observed with the anisotropy ratio ($k_{parallel}/k_{perpendicular}$) ranging between 1.5 and 3.8.

Gas breakthrough experiments

During this study 28 gas breakthrough measurements were performed on 13 rock samples:

(1) seven breakthrough experiments on samples from the Norwegian Shelf (six samples orientated perpendicular and one parallel to bedding)

(2) two breakthrough experiments with nitrogen on Opalinus Clay showing extremely low effective permeability coefficients; a final differential pressure was not reached within the duration of the experiments

(3) 19 gas breakthrough experiments with nitrogen on four Boom Clay samples (four plugs cored parallel and three plugs perpendicular to bedding)

All experiments reported here were carried out with nitrogen. The results of the evaluations of the experiments are listed in Table 6.

Effective permeability coefficients

The effective permeability coefficients (k_{eff}) reported in Table 6 represent the maximum values recorded in the corresponding breakthrough experiment. Most of the values are in the range from 1 to 21 nDarcy (1×10^{-21} m^2–2.1×10^{-20} m^2). Usually, the k_{eff} values are significantly lower than the corresponding absolute permeability coefficients (k_{abs}). Only in one instance (Boom Clay sample 200247; $k_{eff} = 1100$ nDarcy) does the two-phase effective permeability (k_{eff}) exceed the absolute permeability value ($k_{abs} = 550$ nDarcy). The Tertiary mudstones from the Norwegian Shelf have effective permeabilities ranging from 0.01 to 7.7 nDarcy (1×10^{-23}–7.7×10^{-21} m^2) while the Boom Clay covers the range from 2.4 to 1100 nDarcy (2.4×10^{-21}–1×10^{-18}

Table 6 Results of permeability measurements and gas breakthrough experiments on pelitic rocks. k_{abs}: single-phase absolute permeability coefficients measured with water and/or brine; $P_{c,\,residual}$: residual pressure difference at the end of the gas breakthrough experiment; $P_{c,\,initial\,(exp.)}$: initial experimental pressure difference; k_{eff}: effective gas permeability coefficients (maximum values); maximum pore radii of conducting pores and transport porosity derived from spontaneous imbibition curves; roman numbers indicate repeated gas breakthrough experiments on the same sample plug, the average values were used for regressions.

sample no.	orientation w. resp. to bedding	k_{abs} (water) [nDarcy]	k_{abs} (brine) [nDarcy]	$P_{c,\,residual}$ [MPa]	$P_{c,\,initial\,(exp.)}$ [MPa]	k_{eff} [m^2]	k_{eff} [nDarcy]	max. pore size [nm]	ϕ (transport) [%]
2000241–1	perpendicular	4.3	3.4	6.70	18.8	$1.1\cdot10^{-23}$	0.011	8	$7.0\cdot10^{-5}$
2000241–2	parallel	9.3	12.1	0.70	17.5	$7.7\cdot10^{-21}$	7.7	20	$50\cdot10^{-3}$
2000242–1 (average)	perpendicular	30.9	34.9	1.67	5.4	$3.6\cdot10^{-21}$	3.6	44	$2.3\cdot10^{-3}$
(I)				1.40	6.0	$2.2\cdot10^{-21}$	2.2	42	$1.0\cdot10^{-3}$
(II)				1.80	6.5	$1.6\cdot10^{-21}$	1.6	38	$5.5\cdot10^{-4}$
(III)				1.80	3.6	$6.9\cdot10^{-21}$	6.9	53	$2.3\cdot10^{-3}$
2000242–2	perpendicular	19.7	17.1	2.50	9.9	$4.1\cdot10^{-22}$	0.4	21	$5.0\cdot10^{-4}$
2000246–1	perpendicular	9.9	4.9	–	16.2	$(6.6\cdot10^{-26})$	(0.00006)	–	–
2000246–2	perpendicular	3.4	–	–	14.4	$(4.8\cdot10^{-25})$	(0.0005)	–	–
2000247–1	perpendicular	549.6	542.9	0.06	14.0	$1.1\cdot10^{-18}$	1100	260	$1.2\cdot10^{-2}$
2000251–1 (average)	perpendicular	23.5	23.8	1.28	14.2	$3.0\cdot10^{-21}$	3.0	24	$2.5\cdot10^{-3}$
(I)				1.31	14.2	$3.5\cdot10^{-21}$	3.5	26	$2.7\cdot10^{-3}$
(II)				1.24	14.2	$2.4\cdot10^{-21}$	2.4	21	$2.3\cdot10^{-3}$
2000253–1 (average)	parallel	65.6	47.3	0.62	18.7	$2.1\cdot10^{-20}$	21.0	60	$3.0\cdot10^{-3}$
(I)				0.35	17.7	$2.0\cdot10^{-20}$	20.0	70	$2.0\cdot10^{-3}$
(II)				0.89	19.7	$2.2\cdot10^{-20}$	22.0	50	$4.0\cdot10^{-3}$
2000253–2 (average)	parallel	64.3	–	0.84	13.47	$2.13\cdot10^{-20}$	21.3	42	$4.6\cdot10^{-3}$
(I)				0.95	16.4	$2.2\cdot10^{-20}$	22.0	35	$5.5\cdot10^{-3}$
(II)				0.87	12.0	$1.1\cdot10^{-20}$	11.0	47	$1.9\cdot10^{-3}$
(III)				0.69	12.0	$3.1\cdot10^{-20}$	31.0	44	$6.3\cdot10^{-3}$
2000253–3 (average)	perpendicular	17.0	–	1.76	16.8	$2.6\cdot10^{-21}$	2.6	19	$3.8\cdot10^{-3}$
(I)				1.63	16.5	$2.6\cdot10^{-21}$	2.6	18	$4.3\cdot10^{-3}$
(II)				1.89	17.0	$2.6\cdot10^{-21}$	2.6	19	$3.2\cdot10^{-3}$
2000254–1 (average)	perpendicular	22.5	19.8	0.41	12.8	$4.9\cdot10^{-21}$	4.9	27	$9.2\cdot10^{-4}$
(I)				0.22	14.0	$6.3\cdot10^{-21}$	6.3	33	$5.5\cdot10^{-4}$
(II)				0.46	14.4	$2.7\cdot10^{-21}$	2.7	16	$4.0\cdot10^{-4}$
(III)				0.56	10	$5.80\cdot10^{-21}$	5.8	32	$1.8\cdot10^{-3}$
2000254–2 (average)	parallel	36.1	56.1	0.58	14.1	$7.1\cdot10^{-21}$	7.1	47	$1.0\cdot10^{-3}$
average		65.9	76.2	1.28	13.6	$5.1\cdot10^{-20}$	50.5	43	$2.8\cdot10^{-3}$
minimum		3.4	3.4	0.06	3.6	$1.1\cdot10^{-23}$	0.01	8	$7.2\cdot10^{-5}$
maximum		549.6	542.9	6.70	19.7	$1.1\cdot10^{-18}$	1100.0	260	$1.2\cdot10^{-2}$

m^2). Evaluation of the two measurements on the Opalinus clay yielded k_{eff} values lower by several orders of magnitude than those observed for the other samples. These experiments did not result in typical breakthrough curves but a continuous decline in the pressure gradient over an extended period of time (up to 10 weeks). It is very likely that the transport process observed here is not pressure-driven volume flow (Darcy flow) but molecular diffusion of gas in the water-saturated pore space.

Residual differential pressures

Residual differential pressures are in the range from 0.06 to 6.7 MPa, with lowest pore entry pressures for Boom Clay sample 2000247, and the highest value found for a Norwegian Shelf sample cored perpendicular to bedding (2000241–1). Values of the displacement pressures for the Opalinus Clay specimens are not given because final differential pressures were not reached in these experiments over periods of several weeks.

Pore size distributions and total porosity

Pore size distributions calculated from the imbibition data strongly depend on the values for interfacial tension, and wetting angle used for the system gas/water. Data presented in Table 6 refer to pore radii, and total connected porosity values computed with a wetting angle of 0° and interfacial tension values of 50 mN m^{-1}.

Pore radii determined from breakthrough experiments, were predominantly less than 60 nm, with one plug having a pore radius of 260 nm. Mercury injection data indicate prominent pore radii to be 20 nm with a second set of prominent radii between 120 and 723 nm, thus showing a similar pore size distribution as obtained from the gas breakthrough experiments.

The total porosity ($\phi_{(transport)}$) of the connected, gas-saturated pore system at the maximum effective permeability varies between 1.2×10^{-2} and 7.2×10^{-5}%.

Results of gas breakthrough experiments on three different samples are given in Fig. 6(A–C). Shown on the left are the

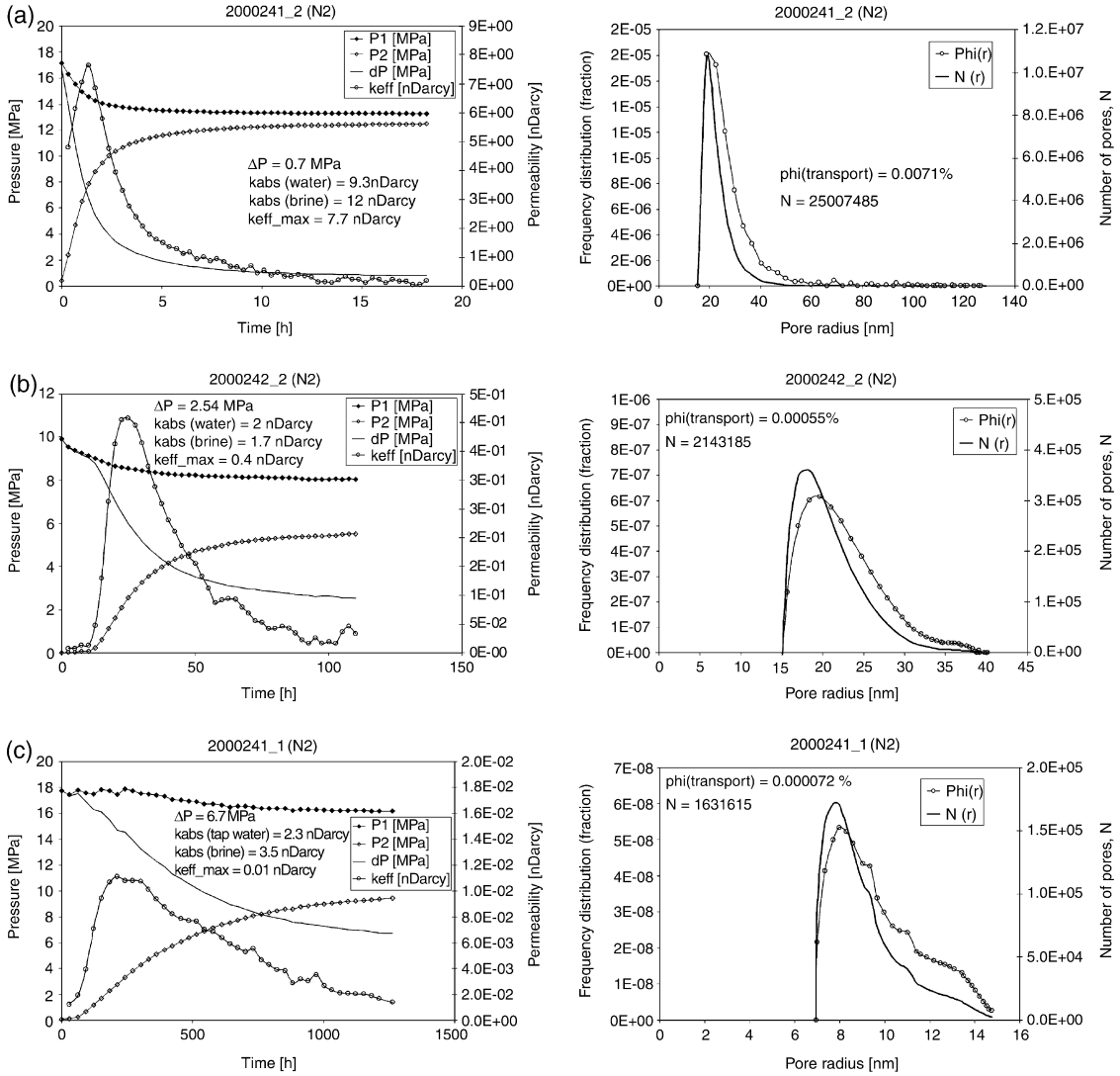

Fig. 6. Experimental results from gas breakthrough measurements on three different mudrock samples. Left: Pressure and effective permeability history versus experimental time. Right: Pore size distributions of conducting pores derived from imbibition curves. P_1 and P_2 are the pressures in the upstream and downstream cell compartments, respectively, *dP* is the instantaneous pressure difference, ΔP is the final differential pressure ('minimum capillary displacement pressure', also referred to as P_d), k_{eff} is the effective permeability to the gas phase; phi(transport) is the total transport porosity for the gas-phase, phi(r) and N(r) are the fractional porosity and number of conducting equivalent pores as a function of the pore radius, respectively. Effective permeabilities of these samples range between 0.7 and 0.01 nDarcy, final differential pressures are in the range of 0.7–6.7 MPa, and total transport porosity ranges from 0.0071 to 0.000072%.

recorded upstream and downstream pressures, the pressure difference and the effective permeability as a function of experimental time. The diagrams on the right show the pore size distributions calculated based on a capillary bundle model, both in terms of fractional porosity and numbers of capillaries.

It is evident that the experimental results exhibit systematic differences in duration (18, 110, and 1300 h). From (A) through (C) the residual pressure differences increase (0.7, 2.5, and 6.7 MPa) while the maximum effective permeability coefficients (7.7, 0.41, and 0.01 nDarcy) decrease and the values of the absolute transport porosity decline from 7×10^{-3} to 7×10^{-5}%.

The data listed in Table 6 show that repeated measurements on the same sample (e.g. residual pressure difference and effective permeability) yield consistent results. An example for the reproducibility of gas breakthrough experiments is given in Fig. 7 for sample 2000251–1.

Correlations

Regressions have been determined for k_{abs}-, maximum k_{eff}-, and $P_{c,\,residual}$-data from 11 sample plugs. The data from the Opalinus Clay samples were not considered because no gas breakthrough was observed. For simplicity and compatibility with results from other studies the residual pressure

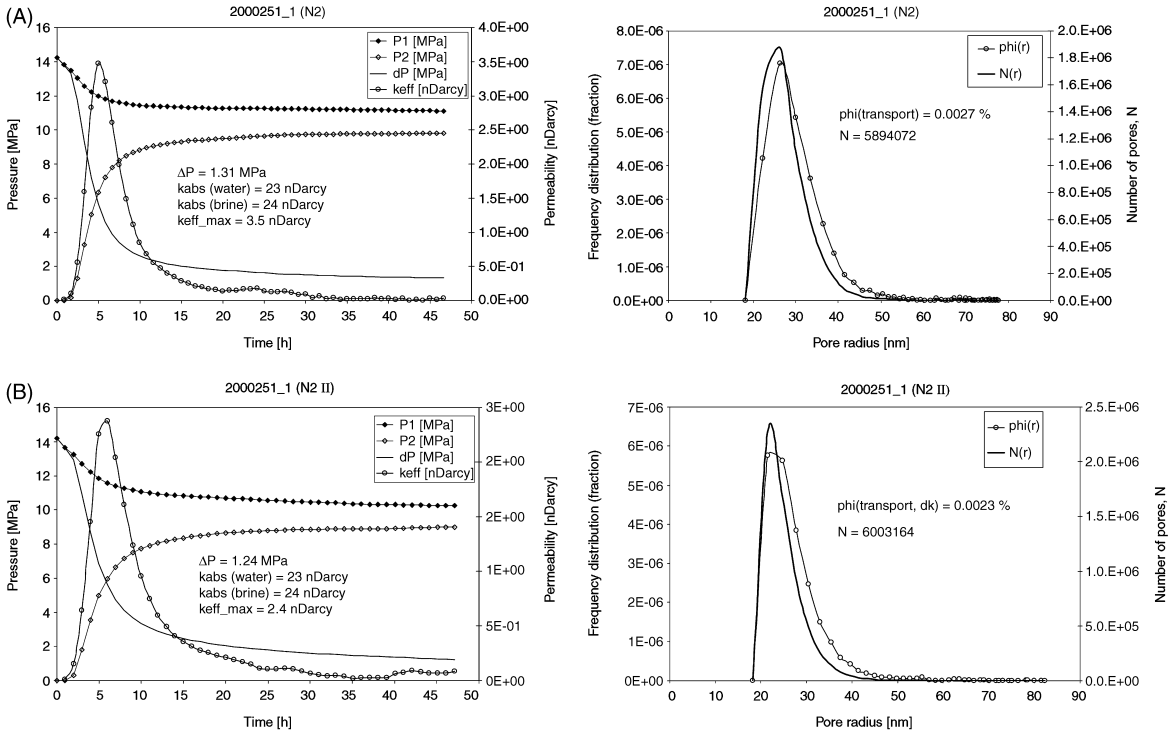

Fig. 7. Results of two gas breakthrough tests conducted on the same sample plug. Diagrams (A) and (B) exemplify the reproducibility of the experiments.

difference was denoted as P_d (displacement pressure) in the diagrams and regression equations. The parameter definitions from the studies referred to are listed in Table 1. Repetitive breakthrough experiments run on the same sample plug are marked by roman numbers in Table 6. For the correlations the results of repetitive runs were averaged.

Figure 8 shows a double-logarithmic plot of the effective (maximum) gas-phase permeability versus absolute permeability. The resulting correlation is:

$$\log(k_{eff}/[\text{nDarcy}]) = 1.9964 \times \log(k_{abs}/[\text{nDarcy}]) - 2.2949 \quad (n = 11)\ R^2 = 0.7922$$

The residual differential pressure (displacement pressure, P_d) was plotted versus absolute permeability in, Fig. 9. Here the following regression equation was obtained:

$$\log(P_d/[\text{MPa}]) = -0.8112 \times \log(k_{abs}/[\text{nDarcy}]) + 1.1549 \quad (n = 11)\ R^2 = 0.7101$$

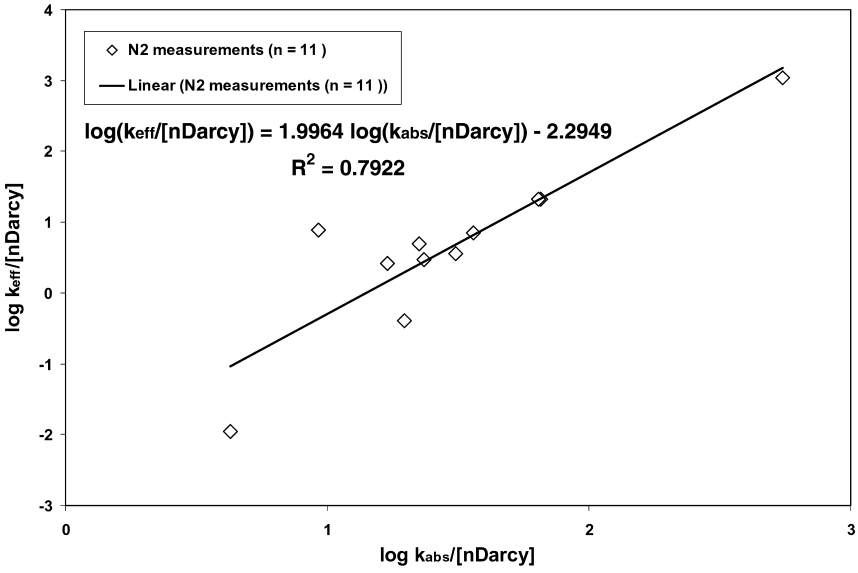

Fig. 8. Plot of effective permeability versus absolute permeability [nDarcy] (this study).

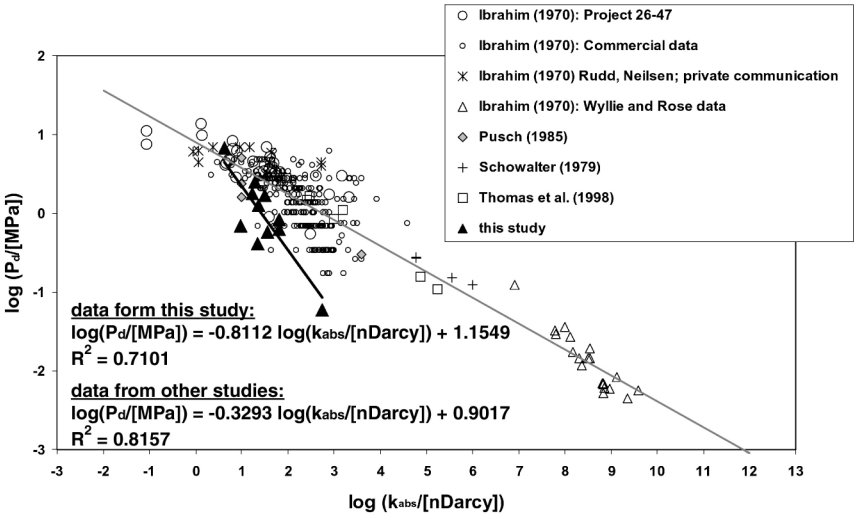

Fig. 9. Comparison of (minimum) capillary displacement pressures (P_d) and absolute permeability coefficients (k_{abs}) of this study with data from other studies.

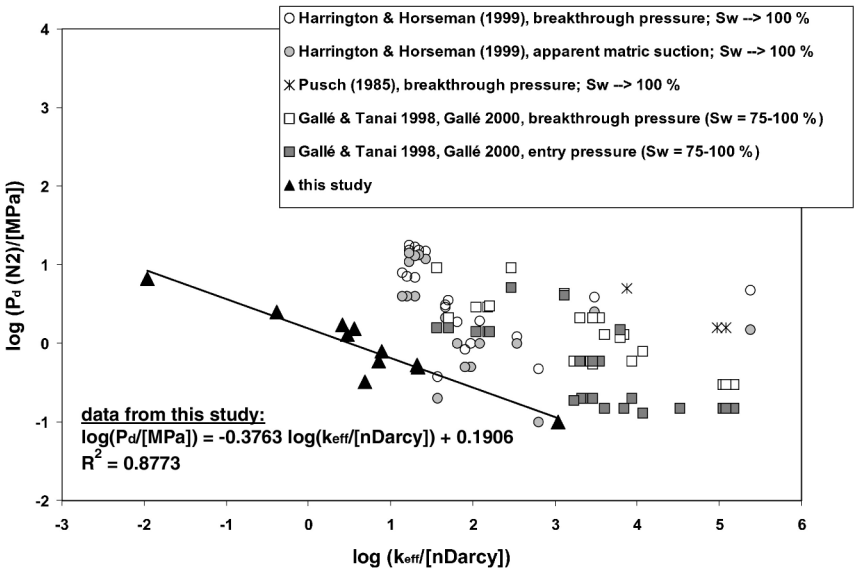

Fig. 10. Comparison of (minimum) capillary displacement pressures (P_d) and effective (gas phase) permeability coefficients (k_{eff}) of this study with data from other studies.

Another correlation could be established between the residual differential pressure (displacement pressure, P_d, Fig. 10) and the effective permeability:

$$\log(P_d/[\,\mathrm{MPa}]) = -0.3997 \times \log(k_{eff}/[\mathrm{nDarcy}]) + 0.218 \quad (n = 11)\ R^2 = 0.8671$$

DISCUSSION

Gas breakthrough experiments reported by Pusch *et al.* (1985), Ibrahim *et al.* (1970), Schowalter (1979), and Gallé (2000) used a stepwise pressure increase or continuous gas pressure build-up (e.g. Horseman *et al.* 1997) until continuous gas or water flow was observed on the downstream side of the samples. The rate of gas-pressure build-up on the high pressure side of the mudstone samples was reported to range between 0.1 and 0.004 MPa h^{-1} (e.g. Pusch *et al.* 1985; Tanai 1997; Harrington & Horseman 1999; Horseman *et al.* 1999). In some instances this rate may have been too rapid to take into account the dynamics (time lag) of the gas breakthrough process (see above).

In contrast to the drainage method, the residual pressure difference ($P_{c,\,residual}$) measured in our imbibition experiments may be lower than the 'true' $P_{c,\,threshold}$ ($P_{c,\,breakthrough}$) value if re-imbition is impeded. While $P_{c,\,threshold}$ corresponds to the first gas breakthrough across a completely water-saturated seal, $P_{c,\,residual}$ will be the characteristic parameter for subsequent (repetitive) breakthrough events across a 'dynamic' seal which has been recurrently breached and then re-sealed by imbibiton. In geological time the latter situation

may be more common in natural gas systems than the former so that the conservative estimate resulting from our method may be more realistic.

The difference between ($P_{c,\,residual}$) and ($P_{c,\,threshold}$) appears to be more significant for samples with higher permeabilities. This could explain the deviation of the trend lines for drainage and imbibition data evident from Fig. 9. Here the capillary displacement pressures (P_d) from our study and from drainage experiments by Pusch *et al.* (1985), Thomas *et al.* 1968), Ibrahim *et al.* (1970), and Schowalter (1979) have been plotted over the corresponding absolute permeability coefficients. At absolute permeabilities above ~100 nDarcy the P_d values from the imbibition experiments tend to be substantially lower than those from the drainage experiments.

Apart from the results of this study the displacement pressure versus effective permeability plot in Fig. 10 shows data from previous studies for comparison. These comprise matric suction values (residual capillary pressures), entry and breakthrough pressures published by Pusch (1985), Gallé & Tanai (1998), Harrington & Horseman (1999), Gallé (2000). The regression analysis of our data reveals a good correlation between P_d and k_{eff}. It is evident, however, that at given effective permeabilities our correlation predicts consistently lower displacement pressures.

Gas migration through the pore system of the clay matrix

Harrington & Horseman (1999) argue that in an initially water-saturated clay with extremely small pores, the capillary displacement pressure is simply too large for the gas to penetrate and desaturate the matrix without fracturing the sample. In the absence of such cracks, normal two-phase flow through the intergranular porosity is considered impossible. The conditions for fracturing depend, however, on the local stress field. Fractures will only form if the pressure required for capillary breakthrough of gas exceeds the minimum principal stress, i.e. the confining pressure ($P_{conf.}$), plus the tensile strength of the rock. Due to the fact that most breakthrough pressures reported by Horseman *et al.* (1997, 1999) and Harrington & Horseman (1999) are close to the experimental confining pressure these authors suggest that hydraulic fracturing of the rock matrix may have occurred in some instances.

In comparison, data from Schlömer (1998) and this study show that gas breakthrough and flow in mudrocks is possible even at gas pressures much lower than fracture pressure or the minimum principal stress (Fig. 11).

Displacement pressure determined by mercury injection

Information on the capillary sealing efficiency of sedimentary rocks is commonly derived from mercury porosimetry (Schowalter 1979; Schlömer & Krooss 1997; Clennell *et al.* 1999; Dewhurst *et al.* 1999). To correlate the results of mercury porosimetry to the hydrocarbon-water system the following equation is used:

$$P_{d(gas/water)} = P_{d(Hg/air)} \frac{(\gamma_{gas} \cdot \cos\theta_{gas})}{(\gamma_{Hg} \cdot \cos\theta_{Hg})} \qquad (3)$$

where $P_{d(gas/water)}$ and $P_{d(Hg/air)}$ are the capillary pressures within the systems hydrocarbon-water and mercury-air, respectively. In the case of methane, $\theta_{\mathrm{methane}} = 0$ and $\gamma_{\mathrm{methane}} = 0.051\,\mathrm{N\,m^{-1}}$ (at 30°C and 15 MPa; Schowalter, 1979). For the mercury–air system an interfacial tension $\gamma_{\mathrm{Hg}} = 0.480\,\mathrm{N\,m^{-1}}$ and a contact angle $\theta_{\mathrm{Hg}} = 141^{\circ}$ were assumed.

While other authors (Thomas *et al.* 1968) report close relationships between displacement pressures from mercury porosimetry data with the results of the gas breakthrough measurements, the present study did not reveal

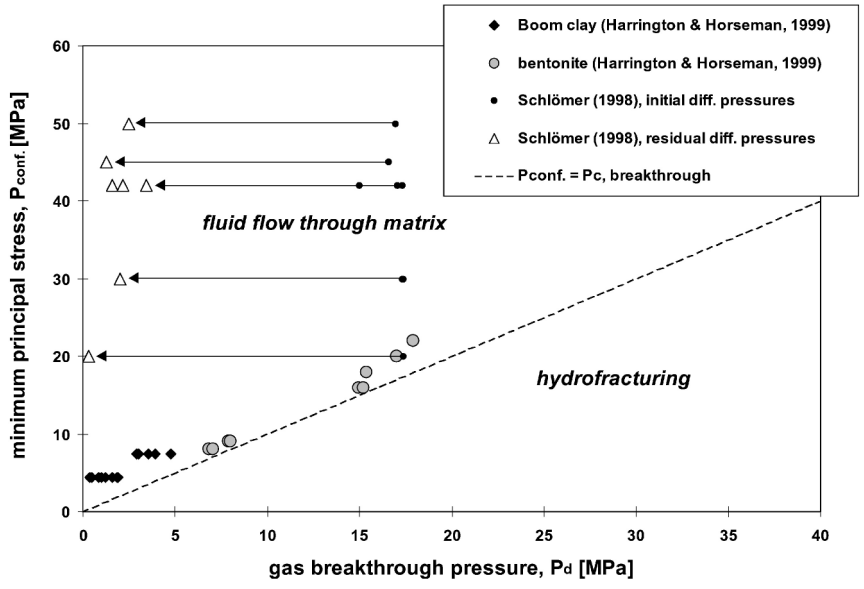

Fig. 11. Plot of the minimum principal stress or confining pressure ($P_{\mathrm{conf.}}$) versus the gas breakthrough pressure ($P_{\mathrm{c\ (breakthrough)}}$) examined by gas breakthrough experiments (Schlömer 1998; Harrington & Horseman 1999).

any correlation between values determined by both techniques. This is in line with results obtained by Schlömer (1998) for fine-grained sedimentary rocks and is a consequence of the fact that the conventional omnidirectional mercury intrusion procedure does not take adequately into account the substantial degree of anisotropy of most mudrocks. Furthermore, as pointed out by Schlömer & Krooss (1997) the interpretation of mercury porosimetry data in terms of capillary breakthrough pressure is to some extent arbitrary. Another critical problem is the sample preparation prior to mercury injection. Samples must be dried at 105°C, which may cause changes in the clay fabric. Due to the loss of structural water within the clay minerals the space between distinct silicate layers may become much smaller. On the other hand, drying may cause larger pore space between distinct aggregates due to shrinkage of clay minerals.

Maximum effective permeability

With respect to the range of initial differential pressures used in breakthrough experiments of this study (3.5–19.7 MPa) the question arises whether the maximum effective permeability depends on the absolute initial value of the differential pressure used, i.e. if higher initial pressure differences result in higher effective permeability values. Due to the strong capillary forces involved it is unlikely, that higher initial differential pressures would result in a substantial decrease of the IRWS (Fig. 5). In consequence only very small additional portions of equivalent pore radii would become accessible for gas transport (e.g. for $\Delta P = 100$ MPa pores of 1 nm diameter, assuming $\gamma = 50\,\mathrm{mN\,m^{-1}}$, $\theta = 0°$), which should not have a significant influence on permeability.

Effect of sample length on capillary breakthrough

Theoretically, capillary breakthrough and the residual pressure difference determined in the experiments reported here should not depend on the length of the sample plug because this pressure strictly depends only on the largest effective pore throat along the flowpath. From a statistical point of view, the probability of occurrence of a flowpath with a capillary threshold pressure significantly lower than the characteristic one will increase as sample length is reduced. For the fine-grained rocks used in this study, a thickness (length) of 1–2 cm is considered sufficient to provide representative threshold pressures.

Transport porosity

Compared with the total porosity of the samples determined by mercury porosimetry (23–29%) extremely small values (down to 7×10^{-5}%) were obtained for the transport porosity, i.e. the nominal fraction of the rock volume corresponding to gas-saturated flow pathways after breakthrough. These values indicate that gas flow occurs in a very localized (focused) fashion along a limited number of interconnected pathways.

Like the pore-size distribution the transport porosity was computed using a simple capillary bundle model. To demonstrate the amount of transport porosity required to account for the observed effective gas permeability values the (equivalent) pore volume of a conducting pore system can be estimated based on Poiseuille's and Darcy's law. Assuming that the permeability coefficient measured for the fluid (gas) transport across a sample of diameter R is accounted for by N cylindrical capillaries of radius r, this radius can be computed according to:

$$r = \sqrt[4]{\frac{8 \cdot k_{eff} \cdot R^2}{N}} \tag{4}$$

Then $n(r/R)^2$ represents the porosity of this equivalent porous medium. Table 7 lists (for $N = 1$ and $N = 100000$) the equivalent pore radii and the porosities of a cylindrical sample with $R = 1.43$ cm for effective permeability values from 10 to 10^{-2} nDarcy (10^{-20}–10^{-23} m^2). For the single capillary case ($N = 1$) equivalent capillary radii range from 2.0 to 0.4 μm and equivalent porosities from 2.0×10^{-8} to 6.3×10^{-1}. Assuming a bundle of 100000 capillaries, equivalent radii range from 1.13×10^{-7} to 2.01×10^{-8} while the equivalent (transport) porosities 6.28×10^{-6}–1.98×10^{-7}.

Pressure-driven volume flow versus molecular diffusion

The extremely low nominal permeability coefficients obtained for the Opalinus samples and the absence of a typical breakthrough characteristics in the recorded pressure data imply that capillary breakthrough did not occur in these experiments and that the observed pressure changes were

Table 7 Equivalent pore radii and porosities ($\phi_{(transport)}$) for a cylindrical rock sample with R = 1.43 cm for effective permeability values (k_{eff}) from 10^{-20} to 10^{-23} m^2. The calculation was done for one single capillary ($N = 1$) with the radius r and for a set of 100000 capillaries with correspondingly smaller radii.

k_{eff} [m^2]	r ($N = 1$) [m]	r ($N = 1$) [μm]	ϕ(transport) [fraction]	r ($N = 100000$) [m]	r ($N = 100000$) [μm]	ϕ(transport) [fraction]
10^{-20}	$2.0 \cdot 10^{-6}$	2.0	$2.0 \cdot 10^{-8}$	$1.13 \cdot 10^{-7}$	0.11	$6.28 \cdot 10^{-6}$
10^{-21}	$1.1 \cdot 10^{-6}$	1.1	$6.3 \cdot 10^{-9}$	$6.35 \cdot 10^{-8}$	0.06	$1.98 \cdot 10^{-6}$
10^{-22}	$6.4 \cdot 10^{-7}$	0.6	$2.0 \cdot 10^{-9}$	$3.57 \cdot 10^{-8}$	0.04	$6.28 \cdot 10^{-7}$
10^{-23}	$3.6 \cdot 10^{-7}$	0.4	$6.3 \cdot 10^{-10}$	$2.01 \cdot 10^{-8}$	0.02	$1.98 \cdot 10^{-7}$

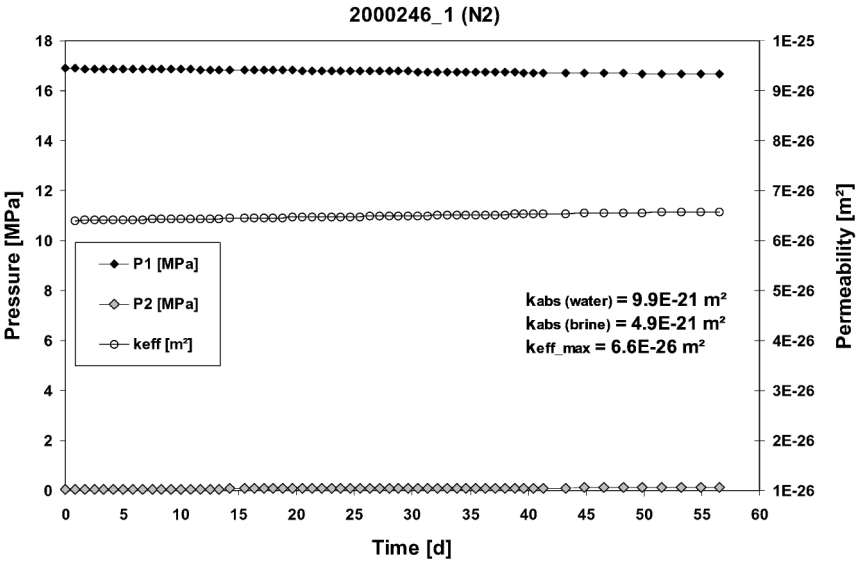

Fig. 12. Gas breakthrough experiment on Opalinus Clay: even a duration of 55 days did not lead to a distinct breakthrough. The effective permeability calculated from the slight pressure decay within the high and low pressure side results in effective permeabilities of $6.6{\cdot}10^{-26}$ m^2.

Table 8 Equivalent permeability estimated from a typical effective diffusion coefficient D (cf. Schlömer & Krooss 1997) across a sample with a given length (Δx), and porosity (ϕ); P1 = upstream side pressure, P2 = downstream side pressure.

N2 solubility in water (50 bar, 50°C)	D	ϕ	Δx	Diffusive flux			*P1*	P_2	Viscosity	$k_{(apparent)}$
[p.p.m.]	[m^2 s^{-1}]	[fraction]	[m]	[g m^{-2} s^{-1}]	[mol m^{-2} s^{-1}]	[Std. m^3 m^{-2} s^{-1}]	[MPa]	[MPa]	[Pa s]	[m^2]
600	$1.0{\cdot}10^{-10}$	0.1	$2.0{\cdot}10^{-2}$	$3.0{\cdot}10^{-7}$	$1.1{\cdot}10^{-8}$	$2.5{\cdot}10^{-10}$	5.1	0.1	$2.5{\cdot}10^{-5}$	$9.9{\cdot}10^{-25}$

due to diffusive transport across the water-saturated pore space of the samples. A computation was performed to estimate the order of magnitude of equivalent permeability coefficients obtained if this diffusive transport process is falsely interpreted in terms of Darcy flow (Fig. 12). The steady-state diffusive flux of nitrogen across a sample of 2 cm thickness was estimated based on effective diffusion coefficients measured in earlier studies (Schlömer & Krooss 1997), the aqueous solubility of nitrogen (O'Sullivan & Smith 1970) and the porosity of the rock sample. The parameters used for this calculation and the results are listed in Table 8. According to this estimation diffusive transport across a water-saturated rock sample with a porosity of 10% will result in a flux rate that corresponds to an apparent permeability coefficient of 10^{-24} m^2 (10^{-3} nDarcy). Evidently, a differentiation between the transport processes of pressure-driven volume flow and molecular diffusion of gas in the water-saturated pore space is no longer possible at this low permeability level.

CONCLUSIONS

The steady and nonsteady state experiments on selected fine-grained sedimentary rocks performed in this study have provided absolute water permeabilities (k_{abs}, ranging from 3 to 550 nDarcy) and maximum effective permeabilities to the gas phase (k_{eff}, 0.01–1100 nDarcy) as well as information on the capillary sealing efficiency (minimum capillary displacement pressure, P_d) for gas. Hydrofracturing of the rock samples during gas breakthrough experiments was avoided by applying confining pressure well above the gas pressures. Thus, the k_{eff} and P_d values reported here can be readily assumed to reflect the intact (unfractured) state of the sample and fluid flow occurred through the matrix pore system. From the experimental results the following relationships between effective and absolute permeability, and between absolute and effective permeability and the corresponding capillary displacement pressures were derived:

(1) effective permeability–absolute permeability

$$\log(k_{eff}/[\text{nDarcy}]) = 1.9964 \times \log(k_{abs}/[\text{nDarcy}]) - 2.2949$$
$$(n = 11)\ R^2 = 0.7922$$

(2) displacement pressure–absolute permeability

$$\log(P_d/[\text{MPa}]) = -0.8112 \times \log(k_{abs}/[\text{nDarcy}]) + 1.1549$$
$$(n = 11)\ R^2 = 0.7101$$

(3) displacement pressure–effective permeability

$$\log(P_d/[\text{MPa}]) = -0.3763 \times \log(k_{eff}/[\text{nDarcy}]) + 0.218$$
$$R^2 = 0.8671$$

The residual pressure differences recorded at the end of the capillary-controlled, spontaneous re-imbibition process are interpreted to represent a good approximation of the

threshold or breakthrough pressure from the drainage process. If re-imbibition is impeded, the residual *imbibition* pressure differences will be lower than the corresponding *drainage* threshold pressures. Comparison of our experimental results with literature data from drainage experiments suggest that this is likely for samples with permeabilities in excess of 100 nDarcy (10^{-19} m^2). Generally, imbibition data will result in conservative estimates (underestimation) of the capillary sealing efficiency.

Although the dependence of experimental threshold pressures (P_d) on sample length was not examined systematically in the imbibition experiments reported here, the overall consistency of data trends suggests it to be irrelevant for fine-grained rocks with the sample lengths (cm scale) used in the present study. Notwithstanding other heterogeneities an upscaling to geological sequences of fine-grained rocks, appears therefore feasible.

Gas breakthrough with subsequent pressure driven volume flow through very tight water-saturated sediments may become impossible and in these instances molecular diffusion will become the dominating transport process. It was shown that for nominal permeability coefficients below 10^{-3} nDarcy (10^{-24} m^2), under the experimental conditions used here, a distinction between pressure driven volume flow and diffusion processes (assuming an effective diffusion coefficient of 10^{-10} m^2 s^{-1} and a sample porosity of 10%) is no longer possible.

The pore-size distribution of the conducting pores can be derived from the dependence of the effective permeability on the pressure gradient. Pore size distribution maxima obtained with this approach range mostly between 20 and 50 nm with values going up to 260 nm. The total porosity of the conducting pore system estimated by a capillary bundle model varies between 10^{-2} and 10^{-5}%.

Outlook

Research on the gas-sealing efficiency of pelitic rocks in our laboratory has recently been extended to carbon dioxide. This compound represents a particular challenge due to its phase behaviour (liquid, gas, supercritical fluid) and its reactivity. Initial results of breakthrough experiments with gaseous CO_2 indicate different permeability/threshold pressure correlations than for nitrogen and methane. Diffusion experiments are being conducted to assess the influence of migrating CO_2 on the properties of seal rocks overlying natural carbon dioxide accumulations.

ACKNOWLEDGEMENTS

We gratefully acknowledge financial support for this study received from Norsk Hydro (Bergen) and EniTechnology (San Donato Milanese). Part of this study was performed under the EU NASCENT Project. Sample material was kindly provided by Norsk Hydro (Sven Hansen & Christian Zwach), the Geological Survey of Belgium (Michiel Dusar) NAGRA (Andreas Gautschi) and Janos Urai (RWTH-Aachen), whom we also thank for stimulating discussions. We thank Dr A. Angabini and R. Mildenberger for their support in sample preparation and conduction of the experiments, and Y. Gensterblum for technical assistance. The final manuscript benefited from the extensive comments and suggestions of the reviewers Steve Horseman (BGS) and Ben Clennell (UFBA).

REFERENCES

Carruthers DJF (1998) Transport modelling of secondary oil migration using gradient-driven inversion percolation techniques. PhD Thesis Heriot-Watt University, Edinburgh.

Clennell MB, Dewhurst DN, Brown KM, Westbrook GK (1999) Permeability anisotropy of consolidated clays. In: *Muds and Mudrocks: Physical and Fluid-Flow Properties* (eds A J Fleet, J H S Macquaker), pp 79–96.Geological Society: Special Publications, London.

Dewhurst DN, Yang Y, Aplin AC (1999) Permeability and fluid flow in natural mudstones. In: *Muds and Mudrocks: Physical and Fluid-Flow Properties* (eds A J Fleet, J H S Macquaker), pp 23–44. Geological Society: Special Publications, London.

Gallé C (2000) Gas breakthrough pressure in compacted Fo-Ca clay and interfacial gas overpressure in waste disposal context. *Applied Clay Science*, **17**, 85–97.

Gallé C, Tanai K (1998) Evaluation of gas transport properties of backfill materials for waste disposal: H_2 migration experiments in compacted Fo-Ca clay. *Clays and Clay Minerals*, **46**, 498–508.

Harrington JF, Horseman ST (1999) Gas transport properties of clays and mudrocks. In: *Muds and Mudrocks: Physical and Fluid-Flow Properties* (eds A J Fleet, J H S Macquaker), pp. 107–24. Geological Society: Special Publications, London.

Horseman ST, Harrington J, Sellin P (1997) Gas migration in MX80 buffer bentonite. *Materials Research Society Symposium Proceedings*, **465**, 1003–10.

Horseman ST, Harrington JF, Sellin P (1999) Gas migration in clay barriers. *Engineering Geology*, **54**, 139–49.

Ibrahim MA, Tek MR, Katz DL (1970) Threshold pressure in gas storage, *Pipeline Research Committee American*. Gas Association at the University of Michigan, Michigan.

Ingram GM, Urai JL, Naylor MA (1997) Sealing processes and top seal assessment. In: *Hydrocarbon Seals* (eds P Møller-Pedersen, A G Koestler). pp 165–74. Norwegian Petroleum Society (NPF). Special Publications, Elsevier, Singapore.

Katz AJ, Thompson AH (1987) Prediction of rock electrical conductivity from mercury injection measurements. *Journal of Geophysical Research*, **92**, 599–607.

Neuzil CE (1994) How permeable are clays and shales? *Water Resources Research*, **30**, 145–50.

O'Sullivan TD, Smith NO (1970) The solubility and partial molar Volume of nitrogen and methane in water and in aqueous sodium chloride from 50 to 125°C and 100–600 atm. *Journal of Physical Chemistry*, **74**, 1460–6.

Odén S (1916) Über die Vorbehandlung der Bodenproben zur mechanischen Analyse. *Bulletin of the Geological Institute University Upsala*, **16**, 136–58.

Pusch R (1983) Gas migration through bentonite. *SKBF/KBS* Technical report 83–71.

Pusch R, Ranhagen L, Nilsson K (1985) Gas migration through MX-80 bentonite. *NAGRA NTB, Technical Report*, **85–36**, 28.

Rodwell WR, Harris AW, Horseman ST, Lalieux P, Müller W, Ortiz-Amaya L, Preuss K (1999) Gas migration and two-phase flow through engineered and geological barriers for a deep repository for radioactive waste. Nuclear Science and Technology, EUR 19122 EN.

Schlömer S (1998) Abdichtungseigenschaften pelitischer Gesteine: Experimentelle Charakterisierung und geologische Relevanz, Berichte des Forschungszentrums Jülich.

Schlömer S, Krooss BM (1997) Experimental characterisation of the hydrocarbon sealing efficiency of cap rocks. *Marine and Petroleum Geology*, **14**, 565–80.

Schowalter TT (1979) Mechanics of secondary hydrocarbon migration and entrapment. *AAPG Bulletin*, **63**, 723–60.

Smith DA (1966) Theoretical considerations of sealing and non-sealing faults. *AAPG Bulletin*, **50**, 363–74.

Tanai K, Kanno T, Gallé C (1997) Experimental study of gas permeabilities and breakthrough pressures in clays. *Materials Research Society Symposium Proceedings*, **465**, 995–1002.

Thomas LK, Katz DL, Tek MR (1968) Threshold pressure phenomena in porous media. *Society of Petroleum Engineers Journ*, **243**, 174–84.

Thury M, Bossart P (1999) Mont Terri Rock Laboratory: Results of the hydrogeological, geochemical and geotechnical experiments performed in 1996 and 1997. *Swiss National Hydrological and Geological Survey (Bern)*.

Tributh H, Lagaly G (1986) Aufbereitung und Identifizierung von Boden- und Lagerstättentonen, 1. Aufbereitung der Proben im Labor, 2. Korngrößenanalyse und Gewinnung von Tonsubfraktionen. GIT Fachzeitschrift für das. *Laboratorium, Kolloidchemie*, **30**, 524–9.

Washburn EW (1921) Note on a method of determining the distribution of pore sizes in a porous material. *Proceedings of the National Acadamy of Science*, 115–116.

Zhang T, Krooss BM (2001) Experimental investigation on the carbon isotope fractionation of methane during gas migration by diffusion through sedimentary rocks at elevated temperature and pressure. *Geochimica et Cosmochimica Acta*, **65**, 2723–42.

APPENDIX A: SYMBOLS

Symbol	Unit	Definition
k	[m^2], [Darcy]	permeability coefficient (1 Darcy = $0.987 \cdot 10^{-12}$ m^2)
k_{abs}	[m^2], [Darcy]	absolute permeability; single-phase flow
k_{eff}	[m^2], [Darcy]	effective permeability; multiphase flow
k_r	[fraction]	relative permeability
Q	[$m^3/m^2/s$]	volume flow of fluid through the porous medium
η	[Pa s]	dynamic viscosity of the permeating fluid
A	[m^2]	cross-sectional area perpendicular to the flow direction
Δx	[m]	sample length
P	[Pa]	pressure
$P_c = \Delta P$	[Pa]	capillary pressure
P_d	[Pa]	capillary displacement pressure
$P_{conf.}$	[Pa]	confining pressure
γ	[N/m]	interfacial tension
θ	[degrees]	wetting angle
V	[m^3]	volume
t	[s]	time
n	[mol]	amount of substance
R	[J mol^{-1} K^{-1}]	universal gas constant
T	[K]	temperature
N	dimensionless	number of tubular parallel capillaries
r	[m]	pore radius
r_{eff}	[m]	effective pore radius, smallest pore throat of flowpath
ϕ	[fraction], [%]	porosity
S_w	[fraction], [%]	water saturation
IRWS	[fraction], [%]	irreducible water saturation
RGS	[fraction], [%]	residual gas saturation
S_o	[m^2 g^{-1}]	specific surface area
D	[m^2 s^{-1}]	effective diffusion coefficient
n	dimensionless	number of data points

APPENDIX B

Computation of mass transport through samples

The evaluation is based on the assumption of the validity of the ideal gas law for the pressure and temperature conditions of the experiment:

$$PV = nRT \quad \Longleftrightarrow \quad n = (PV)/(RT) \tag{B1}$$

An infinitesimal increase of gas pressure ($dP2$) during time dt in the downstream chamber of volume V_2 yields the molar gas flux:

$$\frac{dn}{dt} = \frac{V_2}{R \cdot T}\frac{dP_2}{dt} \quad [\text{mol s}^{-1}] \tag{B2}$$

Darcy's law for compressible media

According to Darcy's law the instantaneous volume flux (Q) of an incompressible medium at a given pressure difference is given by:

$$Q = \frac{1}{A}\frac{dV}{dt} = -\frac{k}{\eta}\frac{dP}{dx} \quad [\text{m/s}] \tag{B3}$$

where V [m^3] is the fluid volume, A [m^2] the cross-sectional area perpendicular to the flow direction, k [m^2] the permeability coefficient or intrinsic permeability, η [Pa·s] is the dynamic viscosity of the permeating fluid, and dP/dx [Pa m^{-1}] is the pore pressure gradient. The parameter Q [$m^3/m^2/s$] is also denoted as the 'Darcy velocity' of the fluid.

Integration of eq. B3 between the positions x_1 and x_2 with the corresponding pressures P_1 and P_2 yoelds Darcy's law for compressible media (i.e. a gas phase), where the conventional volume-based form is then converted to a mass-based form using the ideal gas law:

$$\frac{dn}{dt} = -\frac{k \cdot A}{\eta \cdot R \cdot T}\frac{(P_2^2 - P_1^2)}{2dx} \quad [\text{mol s}^{-1}] \tag{B4}$$

Combining this expression with equation (B2) the (instantaneous) effective permeability is calculated from the gas

pressure change with time in the (downstream) compartment of volume V_2 by the following equation:

$$\frac{dn}{dt} = \frac{V_2}{R \cdot T}\frac{dP_2}{dt} = -\frac{k \cdot A}{\eta \cdot R \cdot T}\frac{(P_2^2 - P_1^2)}{2\Delta x}$$
$$\Longleftrightarrow k = -\frac{V_2 \cdot \eta \cdot 2\Delta x}{A(P_2^2 - P_1^2)}\frac{dP_2}{dt}\ [\mathrm{m}^2] \qquad \text{(B5)}$$

A corresponding expression can be derived to compute the permeability coefficient from the pressure decline in a confined upstream compartment.

Pore volume distribution of conducting pores

If the fluid-conducting pore system of the natural rock samples is interpreted in terms of an equivalent pore system of tubular capillaries, the experimental data can be used to derive a pore-volume distribution.

Darcy's law for fluid flow in porous media is given by

$$\frac{Q}{A} = -\frac{k \cdot \Delta P}{\Delta x \cdot \eta}\left[\frac{\mathrm{m}}{\mathrm{s}}\right] \qquad \text{(B6)}$$

where Q/A denotes the volume flux, k is the permeability coefficient [m^2], Δx is the distance [m], ΔP the pressure difference [Pa] and η the viscosity of the fluid [Pa s].

Poiseuille's law for fluid flow in a single capillary of radius r [m] and length Δx is

$$Q = -\frac{r^4 \pi \Delta P}{8\eta \Delta x}\left[\frac{\mathrm{m}^3}{\mathrm{s}}\right] \qquad \text{(B7)}$$

For a bundle of N tubular parallel capillaries arranged over a cross-section area A the volume flux per unit of bulk cross section area (Q/A) is given by:

$$\frac{Q}{A} = -\frac{N \cdot r^4 \cdot \pi \cdot \Delta P}{A \cdot 8 \cdot \Delta x \cdot \eta}\left[\frac{\mathrm{m}}{\mathrm{s}}\right] \qquad \text{(B8)}$$

The ratio of the pore volume $N \cdot r^2 \cdot \pi \cdot \Delta x$ and the bulk volume $A \cdot \Delta x$ of the capillary arrangement is its porosity:

$$\phi = \frac{N \cdot r^2 \cdot \pi \cdot \Delta x}{A \cdot \Delta x} \qquad \text{(B9)}$$

Combination of (B6) (B8) and (B9) yields the relationship:

$$\phi = \frac{8k}{r^2} \qquad \text{(B10)}$$

According to this equation an arrangement of capillaries of equal radius r and a permeability coefficient k corresponds to a defined porosity value ϕ (volume fraction $V_{capillary}/V_{bulk}$ within the system along which fluid transport occurs).

This relationship contains material properties of the porous medium and the equivalent capillary arrangement and is essentially independent of the medium (compressible or incompressible) used to determine the permeability. Effects resulting from slip flow, Knudsen diffusion or the Klinkenberg effect are not considered here.

A porous medium typically has a specific pore-size distribution. Different groups of pores are accessible for the nonwetting phase depending on the pressure difference between the two fluid phases. Consequently the permeability of the initially water-saturated porous samples varies as a function of gas pressure gradient. During the drainage process each pressure increase will add to the conducting pore system a new set of capillaries of a distinct porosity ϕ and permeability k. Thus, the maximum effective gas permeability value determined in our experiments is the cumulative permeability coefficient, corresponding to a gas flow through various sets of capillary pathways with different equivalent diameters extending from the diameter of the largest interconnected pathways to the diameter of the smallest pores accessible to gas at the corresponding differential pressure. The decrease in permeability observed during re-imbibition of water, will initially affect the smallest gas-filled pores and extend to the larger pores as the pressure difference continues to decrease. Proceeding from a tubular capillary arrangement of porosity ϕ to an arrangement with porosity $\phi_{(r)} - \mathrm{d}\phi_{(r)}$ involves a corresponding infinitesimal change in permeability ($dk_{(r)}$) and capillary radius (dr), and rewriting equation (B 10):

$$\frac{d\phi_{(r)}}{dr} = \frac{8}{r^2}\frac{dk_{(r)}}{dr} \qquad \text{(B11)}$$

where the capillary radius is directly related to the capillary pressure by the Washburn equation. This equation represents the pore volume distribution of the conducting pores, i.e. the change in the volume fraction of conducting pores as a function of the pore radius accessible for gas flow. Here the interfacial tension and the wetting angle are assumed constant.

Integration of equation (B11) between the largest (r_{max}) and the smallest (r_{min}) pore radius accessible for gas transport yields the total fractional volume of the conducting or transport pore system ($\phi_{(transport)}$):

$$\int_{r\,\mathrm{min}}^{r\,\mathrm{max}} d\phi_{(r)}\,dr = 8\int_{r\,\mathrm{min}}^{r\,\mathrm{max}} \frac{dk_{(r)}}{r^2}\,dr \qquad \text{(B12)}$$